The Removal of Sulfamonomethoxine (SMM) with Copper oxide/Zirconium dioxide (CuO/ZrO_2) Nanocomposites by Photocatalytic Degradation in Pharmaceutical Industry Wastewaters and the Evaluation of Microtox (*Aliivibrio fischeri*) and *Daphnia magna* Acute Toxicity Assays

ABSTRACT

In this study, Copper oxide/zirconium dioxide (CuO/ZrO_2) nanocomposites (NCs) as a photocatalys was examined during photocatalytic degradation process in the efficient removal of Sulfamonomethoxine (SMM) from pharmaceutical industry wastewater plant, İzmir, Turkey. Different pH values (3.0, 4.0, 7.0, 9.0, 10.0 and 12.0), increasing SMM concentrations (5 mg/l, 10 mg/l, 20 mg/l and 40 mg/l), increasing CuO/ZrO_2 NCs concentrations (100 mg/l, 200 mg/l, 400 mg/l, 800 mg/l and 1000 mg/l), different CuO/ZrO_2 NCs mass ratios (1/2, 2/3, 3/4, 4/4, 4/3, 3/2, 2/1), increasing recycle times (1., 2., 3., 4., 5., 6. and 7.) was operated during photocatalytic degradation process in the efficient removal of SMM in pharmaceutical industry wastewater. The characteristics of the synthesized nanoparticles (NPs) were assessed using X-Ray Difraction (XRD), Diffuse Reflectance UV-Vis spectra (DRS), Field Emission Scanning Electron Microscopy (FESEM), Energy-Dispersive X-Ray (EDX), Fourier Transform Infrared Spectroscopy (FTIR), Transmission Electron Microscopy (TEM) and X-Ray Photoelectron Spectroscopy (XPS) analyses, respectively. The acute toxicity assays were operated with Microtox (*Aliivibrio fischeri* also called *Vibrio fischeri*) and *Daphnia magna* acute toxicity tests. The photocatalytic degradation mechanisms of CuO/ZrO_2 NCs and the reaction kinetics of SMM were evaluated in pharmaceutical industry wastewater during photocatalytic degradation process. Cost analysis was evaluated for SMM removal with CuO/ZrO_2 NCs by photocatalytic degradation process in pharmaceutical industry wastewater. ANOVA statistical analysis was used for all experimental samples. The maximum 99.6% SMM removal efficiency was obtained during photocatalytic degradation process in pharmaceutical industry wastewater, at 350 W UV-vis light irradiation power, at 147 mW/cm^2 light intensity, after 120 min photocatalytic degradation time, at pH=12.0 and at 25^oC, respectively. The maximum 99.2% SMM removal efficieny was found with photocatalytic degradation process in pharmaceutical industry wastewater, at 5 mg/l SMM, at 350 W UV-vis, at 147 mW/cm^2, after 120 min, at pH=12.0 and at 25^oC, respectively. The maximum 99.5% SMM removal efficieny was measured to 800 mg/l CuO/ZrO_2 NCs with photocatalytic degradation process in pharmaceutical industry wastewater, at 5 mg/l SMM, at 350 W UV-vis, at 147 mW/cm^2, after 120 min, at pH=12.0 and at 25^oC, respectively. The maximum 99.4% SMM removal efficiency was measured at 4/3wt CuO/ZrO_2 NCs mass ratios, at 5 mg/l SMM, at 800 mg/l CuO/ZrO_2 NCs, at 350 W UV-vis, at 147 mW/cm^2, after 120 min, at pH=12.0 and at 25^oC, respectively. The maximum 99.5% SMM recovery efficiency was measured in pharmaceutical industry wastewater during photocatalytic degradation process, after 1. recycle time, at 5 mg/l SMM, at 800 mg/l CuO/ZrO_2 NCs, at 4/3wt CuO/ZrO_2 NCs mass rartio, at 350 W UV-vis, at 147 mW/cm^2, after 120 min, at pH=12.0 and at 25^oC, respectively. 97.31% maximum Microtox (*Aliivibrio fischeri*) acute toxicity removal yield was found in SMM=20 mg/l after 180 min photocatalytic degradation time, and at 60^oC. It was observed an inhibition effect of SMM=40 mg/l to Microtox with *Vibrio fischeri* after 180 min, and at 60^oC. 93.27% maximum *Daphnia magna* acute toxicity removal was obtained in SMM=20 mg/l after 180 min, and at 60^oC, respectively. It was obtained an inhibition effect of SMM=40 mg/l to *Daphnia magna* after 180 min and at 60^oC. Increasing the SMM concentrations from 5 mg/l to 40 mg/l did not have a positive effect on the decrease of EC_{50} values. SMM concentrations > 20 mg/l decreased the acute toxicity removals by hindering the photocatalytic degradation process. Similarly, a

significant contribution of increasing SMM concentration to acute toxicity removal at 60^{o}C after 180 min of photocatalytic degradation time was not observed. Low toxicity removals found at high SMM concentrations could be attributed to their detrimental effect on *Aliivibrio fischeri* and *Daphnia magna*. As a result, the CuO/ZrO_2 NCs photocatalyst during photocatalytic degradation process in pharmaceutical industry wastewater was stable in harsh environments such as acidic, alkaline, saline, and then was still effective process. When the amount of contaminant was increased, the a novel CuO/ZrO_2 NCs photocatalys during photocatalytic degradation process performance was still considerable. The synthesis and optimization of CuO/ZrO_2 heterostructure photocatalyst provides insights into the effects of preparation conditions on the material's characteristics and performance, as well as the application of the effectively designed photocatalyst in the removal of antibiotics, which can potentially be deployed for purifying wastewater, especially pharmaceutical wastewater. Finally, the combination of a simple, easy operation preparation process, excellent performance and cost effective, makes this CuO/ZrO_2 NCs a promising option during photocatalytic degradation process in pharmaceutical industry wastewater treatment.

Keywords: ANOVA statistical analysis; Antibiotics; Copper oxide/zirconium dioxide (CuO/ZrO_2) nanocomposites (NCs); Cost analysis; Diffuse reflectance UV-Vis spectra (DRS); Energy-dispersive X-ray (EDX); Field emission scanning electron microscopy (FESEM); Fourier transform infrared spectroscopy (FTIR); Hydroxly ($OH^{\bullet}$) radicals; Microtox (*Aliivibrio fischeri or Vibrio fischeri*) and *Daphnia magna* acute toxicity tests; Nanoparticles (NPs); Pharmaceutical industry wastewater; Photocatalytic degradation mechanisms; Reaction kinetics; Sulfamonomethoxine (SMM); Sulfonamide antibiotics (SAs); Transmission Electron Microscopy (TEM); Ultraviolet (UV); X-ray difraction (XRD); X-Ray Photoelectron Spectroscopy (XPS).

1. INTRODUCTION

Emerging contaminants (ECs), sometimes known as contaminants of emerging concern (CECs) can refer to a wide variety of artificial or naturally occurring chemicals or materials that are harmful to human health after long-term disclosure. ECs can be classified into several classes, including agricultural contaminants (pesticides and fertilizers), medicines and antidote drugs, industrial and consumer waste products, and personal care and household cleaning products (Idham et al., 2017; Idham et al., 2021). Antibiotics are one of the ECs that have raised concerns in the previous two decades because they have been routinely and widely used in human and animal health care, resulting in widespread antibiotic residues discharged in surface, groundwater, and wastewater.

Antibiotics, which are widely utilized in medicine, poultry farming and food processing (Arenas and Melo, 2018; Pellerito et al., 2018), have attracted considerable attention due to their abuse and their harmful effects on human health and the ecological environment (Fridkin et al., 2014; Tamma et al., 2017). The misuse of antibiotics induces Deoxyribonucleic Acid (DNA) contamination and accelerates the generation of drug-resistant bacteria and super-bacteria (Huo, 2010; Ferri et al., 2017; Tan et al., 2018); thus, some diseases are more difficult to cure (Tong et al., 2018). A number of studies have revealed that the level of antibiotics in the soil, air and surface water, and even in potable water, is excessive in many areas (Alygizakis et al., 2016; Casanova and Sobsey, 2016; Zhang et al., 2016), which will ultimately accumulate in the human body via drinking water and then damage the body's nervous system, kidneys and blood system. Therefore, it is necessary to develop an efficient method to remove antibiotics present in pharmaceutical industry wastewater.

The uncontrolled, ever-growing accumulation of antibiotics and their residues in the environment is an acute modern problem. Their presence in water and soil is a potential

hazard to the environment, humans, and other living beings. Many therapeutic agents are not completely metabolized, which leads to the penetration of active drug molecules into the biological environment, the emergence of new contamination sources, the wide spread of bacteria and microorganisms with multidrug resistance (Jiménez-Totozintle et al., 2018; Kerrigan, et al., 2018; McConnell et al., 2018). Modern pharmaceutical wastewater facilities do not allow efficient removal of antibiotic residues from the environment (Karthikeyan and Meyer, 2006; Dinh et al., 2017), which leads to their accumulation in ecological systems (Dong et al., 2016; Siedlewicz et al., 2018). Global studies of river pollution with antibiotics have shown that 65% of surveyed rivers in 72 countries on 6 continents are contaminated with antibiotics (Barry, 2019). According to the World Health Organization (WHO), surface and groundwater, as well as partially treated water, containing antibiotics residue and other pharmaceuticals, typically at < 100 ng/l concentrations, whereas treated water has < 50 ng/l concentrations, respectively (Maycock and Watts, 2011). However, the discovery of ECs in numerous natural freshwater sources worldwide is growing yearly. Several antibiotic residues have been reported to have been traced at concentrations greater than their ecotoxicity endpoints in the marine environment, specifically in Europe and Africa (Fekadu et al., 2019). Thus, the European Union's Water Framework Directive enumerated certain antibiotics as priority contaminants (Wang et al., 2017a; Wang et al., 2017b; Wang et al., 2017c). In some rivers, the concentrations were so high that they posed a real danger to both the ecosystem and human health. This matter, the development of effective approaches to the removal of antibiotics from the aquatic environment is of great importance.

The removal of antibiotics and their residues from water and wastewater prior to their final release into the environment is of particular concern (Yang et al., 2021). Modern purification methods can be roughly divided into the following three categories depending on the purification mechanism: biological treatment (Akyon et al., 2019; Zhang et al., 2019), chemical degradation (de Souza Santos et al., 2015; Yang et al., 2021), and physical removal. Each of these methods has its own advantages and disadvantages. For example, biological purification can remove most antibiotic residues, but the introduction of active organisms into the aquatic environment can upset the ecological balance. Various chemical approaches (ozonation, chlorination, and Fenton oxidation) cannot provide complete purification and, in some cases, lead to the death of beneficial microorganisms due to low selectivity. Photocatalysis is widely used in new environmental control strategies (Zhong et al., 2018; Alagha et al., 2021; Yang et al., 2022). However, this method has a number of key disadvantages, such as insufficient use of visible light, rapid annihilation of photogenerated carriers, and incomplete mineralization, which greatly limits its application (Yang et al., 2021).

Sulfonamide antibiotics (SAs) are synthetic antimicrobials derived from sulfanilic acid. Sulfamonomethoxine (SMM) is a SAs. The chemical structure of SAs is characterized by a common sulfanilamide group and a distinct five- or six-member heterocyclic ring (Hu et al., 2007). The SAs have a wide spectrum of antimicrobial action against most gram-positive and numerous gram-negative microorganisms. They inhibit the proliferation of bacteria by acting as the competitive inhibitors of p-aminobenzoic acid in the folic acid metabolism cycle (Sukul and Spiteller, 2006). SAs are widely used in animal husbandry, and account for a high proportion of the total usage of antibiotics in animal therapy. However, SAs exhibit high excretion rates in the urine and feces of medicated animals as parent compounds or metabolites (Thiele-Bruhn, 2003), and are transferred easily from contaminated sites to surrounding waters because of their low sorption to soil and sediments (Sukul and Spiteller, 2006; Sukul et al., 2008). The lack of appropriate treatment for wastewater from farms for removing SA residues has resulted in the residues reaching the receiving waters surrounding the animal farms (Barber et al., 2009; Ryan et al., 2011). The SA residues have been detected

in numerous aquatic environments including fish farms (Le and Munekage, 2004; Dietze et al., 2005), their effluents and downstream waters (Lin et al., 2008; García-Galan et al., 2010a; Luo et al., 2011), rivers (Tamtam et al., 2008; Tamtam et al., 2011), lakes, groundwater (Batt et al., 2006; García-Galan et al., 2010b), and sewage wastewater (Hu et al., 2007; Camacho-Munoz et al., 2014). The spread of SA residues in aquatic environments has generated great concern because of the potential risks such as enhancing microbial resistance through the prolonged exposure of microorganisms to SAs (Kim and Aga, 2007). Furthermore, certain SAs in aquatic environments are potentially toxic to aquatic organisms (Baran et al., 2006).

The impetus of choosing SMM as the target contaminant stems from the fact that SMM is one of the most popular-used pharmaceuticals used for personal care products (PPCPs) but can cause serious environmental pollutions (Littlefield et al. 1989; Littlefield et al. 1990; Reel et al. 1992). The facile, effective, and environment-friendly degradation of SMM-contained wastewater by a UV (365 nm)/Oxone oxidative process is reported, with presenting detailed investigations on the effects of pH values, concentrations of reagents, and reaction time within the treatment process (Pi et al., 2013). 96.78% removal efficiency was found at 5 mg/l SMM, 365 nm wavelenght after 90 min photocatalytic degradation time, respectively (Pi et al., 2013). 100% removal yield was measured at 0.06 mM SMM, at 2.5 mM Fe_3O_4 catalyst after 15 min photocatalytic degradation time, respectively (Yan et al., 2011). 98.5% photocatalytic degradation and 99% COD removal yields were observed at 4.53 mg/l SMM, at 0.49 mmol/l H_2O_2, at 19.51 µmol/l Fe(II), at pH=4.0 after 120 min photocatlaytic degradation time, respectively (Hui et al., 2012). In a research by Zhu et al. (2003), iron oxide magnetic nanoparticles (Fe_3O_4 MNPs) were used to activate persulfate anions ($S_2O_8^{-2}$) to produce sulfate free radicals ($SO_4^{-\bullet}$), which are a powerful oxidant with promising applications to degrade organic contaminants. The kinetics of SMM degradation was studied in the system of Fe_3O_4 MNPs and $S_2O_8^{-2}$. The authors reported a complete removal of the added SMM (0.06 mM) within 15 min with the addition of 1.20 mM $S_2O_8^{-2}$ and 2.40 mM Fe_3O_4 MNPs. There was an optimum concentration of Fe_3O_4 MNPs because Fe_3O_4 MNPs may also act as a $SO_4^{-\bullet}$ scavenger at higher concentrations. Degradation mechanism of SMM on the basis of identification of the degradation intermediates was studied with liquid chromatography combined with mass spectroscopy (LC-MS) (Yan et al., 2011).

Generally, the advanced oxidation processes (AOPs), such as the Fenton or Fenton-like reaction, ozonation or catalytic ozonation, photocatalytic oxidation, electrochemical oxidation, and ionizing radiation, have been widely used for antibiotics degradation in recent years (Anjali and Shanthakumar, 2019; Liu et al., 2020; Wang and Zhuan, 2020; Liu et al., 2021a; Liu et al., 2021b). One of the most promising techniques applied for efficient degradation of antibiotics are Advanced Oxidation Processes (AOPs) (Homem and Santos, 2011; Bagheri et al., 2017; Cuerda-Correa et al., 2020; Lima et al., 2020; Wang and Zhuan, 2020). Nowadays, particular attention is paid to photocatalytic reactions, in which highly oxidizing species responsible for mineralization of organic pollutants are formed in-situ in the reaction media by means of light and a photocatalyst (Homem and Santos, 2011; Biancullo et al., 2019; Wang and Zhuan, 2020; Wei et al., 2020). The photocatalytic activity is closely related to the physicochemical properties but also to the morphology and texture of the materials studied, for this reason the synthesis techniques are often of great importance. Photocatalysis, which occurs under exposure to UV light, is also a common method for the environmental pollutant elimination (Ahmed et al., 2014). The conventional photocatalysis utilizes mostly UV from sunlight, which accounts for only 4% of the solar energy. Therefore, through the introduction of catalysts, the utilization rate of sunlight can be effectively improved. To overcome the low-efficiency problem of the photocatalysis, the development of a more efficient catalyst system that would effectively improve the catalytic oxidation efficiency and overcome the existing limitations is important. The catalytic activity of the

catalyst can be effectively improved by modulating its surface area, preparation method, and changing its properties and structures (Wang et al., 2014; Ren et al., 2015; Mady et al., 2019; Zhu et al., 2020).

Numerous materials have been reported to have the potential and capacity to treat water or wastewater polluted with these antibiotics residue by applying the processes of adsorption and catalytic oxidation during the last few decades. The reported materials include mesoporous carbon beads (Ahammad et al., 2021), biochar (Li et al., 2017a Li et al., 2017b; Jiang et al., 2020; Shirani et al., 2020), clay minerals (Ahmed et al., 2015), activated carbon (Zhang et al., 2020a; Zhang et al., 2020b; Avcu et al., 2021; Ji et al., 2022), cellulose (Shahnaz et al., 2021; Wang et al., 2021), and chitosan (Cui et al., 2019; Phasuphan et al., 2019; ALOthman et al., 2020). As a result of engineering and science evolution, and in complement to the urgent need to increase the adsorption capability of antibiotic contaminants, more advanced materials such as carbon nanotube (CnT) (Yu et al., 2016; Zhao et al., 2016; Bellamkonda et al., 2019; Rigueto et al., 2021), nano-zero valent iron (nZVI) (Ahmed et al., 2017; Zhao et al., 2020; Nguyen et al., 2020; Nyugen et al., 2021; Falyouna et al., 2022a; Falyouna et al., 2022b), nanoporous carbons (Mokhati et al., 2021), porous graphene (Shan et al., 2017; Khalil et al., 2020) and graphene oxide (GO) (Görmez et al., 2019; Qiao et al., 2020; Idham et al., 2021; Nguyen et al., 2021), to date have been analyzed and improved in their ability to remove these ECs from water.

Nanomaterials with a high specific surface area are a promising platform for the development and production of low-cost and highly efficient sorbents for various pollution molecules (Yadav et al., 2021; Liu et al., 2022). For example, graphene-based nanomaterials were utilized to remove antibiotics (Bao, et al., 2018; Tang et al., 2019; Wang et al., 2019a; Wang et al., 2019b), which are adsorbed on the material surfaces due to π-π-, electrostatic or hydrophobic interactions, as well as the formation of hydrogen bonds. Highly efficient antibiotic sorption was also observed when using highly porous, surface-active, and structurally stable silica-based materials (Masoudi et al., 2019; Zeidman et al., 2020), metal oxide NPs (Alagha et al., 2021; Sturini et al., 2021; Li et al., 2022), and metal-organic frameworks (Dehghan et al., 2019; Sun et al., 2021a; Sun et al., 2021b). The photocatalysts, which mainly rely on the production of highly oxidizing species such as hydroxyl radical ($OH^{\bullet}$) and superoxide anion radical ($O_2^{-\bullet}$), have been considered an effective approach for the degradation of antibiotics in water (Luo et al., 2015; Lu et al., 2019; Lu et al., 2020; Yu et al., 2020; Chen et al., 2022).

Copper oxide (CuO), a p-type semiconductor with a constrained band gap (1.2-2.0 eV) and a foundation for many high-temperature superconductors and giant magnetoresistance materials, has attracted a lot of attention in recent years (Długosz et al., 2020; Sohail et al., 2021). One of the attractive features of CuO nanoparticles (NPs) is that by controlling its shape and size, optical properties can be controlled. This feature is very important because it directly affects photocatalyst features. This gives importance to CuO synthesis methods because applied synthesis methods can be lead to different shapes and sizes (Sahu et al., 2019; Karuppannan et al., 2021; Majumdar and Ghosh, 2021). Optical properties play an important role in the photocatalyst process, so here the optical properties of CuO NPs are investigated in more detail. CuO NPs have the unique ability to regulate the possible energy levels of CBs and VBs, as well as the bandgap, by adjusting the size and shape of CuO NPs. The band gap in CuO NPs is blue-shifted than bulk CuO NPs. As a result, for wider bandgap nanostructured CuO NPs samples exhibiting absorption in the UV field, CuO photocatalyst exhibits strong absorption in the visible spectrum with a little transparency (Aslani et al., 2011; Jung et al., 2011; Dhineshbabu et al., 2015; Boltaev et al., 2019; Alhazime, 2020). Various techniques have been used to improve the photocatalytic properties of CuO NPs such as NCs formation, binary and ternary heterojunction formation, Z-scheme based photocatalytic system,

introducing of different metal ions as dopants, and coupling with carbonaceous materials (Iqbal et al., 2017; Gerawork, 2020; Raizada et al., 2020; Aadil et al., 2021; Abul Kareem Alghurabi et al., 2021; Rachna et al., 2021).

Zirconium dioxide (or Zircania, ZrO_2) as broad bandgap (3.25–5.1 eV) semiconductor has been widely explored due to the presence of a large number of O_2 vacancies on the surface, significant ion exchange ability and physiochemical stability (Pirzada et al., 2015). ZrO_2 NPs possesses a high value of the dielectric constant, tensile strength, melting and boiling point, however, its wide band gap and low separation rate of photogenerated electron and hole hinder the wide-scale applications (Aldeen et al., 2022). To overcome this, various enhancement strategies like doping, heterojunction formation incorporation of cocatalysts, etc., have been potentially explored. For instance, Co doped ZrO_2 NCs synthesized by facile-chemical precipitation showed greater degrading activity against methylene blue dye when exposed to visible light due to the improved dielectric properties (Ahmed and Iqbal, 2020). Therefore, coupling ZrO_2 NPs with narrow band semiconductors like MoS_2, TiO_2 and g-C_3N_4 also retards the photocarrier reassembly and augments its photocatalytic performance (Zhang et al., 2020c). The optical properties of ZrO_2 NPs can be enhanced by introducing new electronic states by doping with rare earth metals. For example, the introduction of Ce (IV) ions in ZrO_2 NPs enhanced the photoresponse through the formation of midgap states and the Ce 4f empty states acted as a electron transfer bridge between valence band (VB) and conduction band (CB) of ZrO_2 NPs by low energy photons (García-López et al., 2018). Recent research has manifested that zirconia-based materials show high redox abilities, large surface area, and low thermal conductivity in photocatalytic processes. In this regard, Aldeen et al. (2022), comprehensively explored the altered ZrO_2 NPs based photocatalysts for organic pollutant degradation. The typical insights of inorganic pollutant degradation, specifically the heavy metal ions present in waste water, are missing. Additionally, the importance of generating O_2 vacancies (OVs) in ZrO_2 NPs for the synergistic improvement in opto-electronic properties still needs further comprehension. Hence, the present review article highlights the features of ZrO_2 NPs semiconducting material for the photocatalytic removal of organic as well as inorganic pollutants present in wastewater. Starting from the optimal crystal structure of ZrO_2 NPs, various phases and the subsequent photocatalytic features are comprehensively reviewed. Significant methods to circumvent the inherent drawbacks of the bare ZrO_2 photocatalyst have been inclusively illustrated using different methods such as doping, heterojunction formation, morphology, and structural modulation along with the formation of OVs. After this, the review introduces facile synthesis routes involving bottom-up (solvothermal, Morphology control, and doping) and top-down methods (ultrasonication and chemical reduction) to design ZrO_2-based photocatalytic materials. Then, in order to highlight the advancement of ZrO_2 as a photocatalyst, the mechanistic insights of wastewater treatment via photocatalysis of organic and inorganic pollutants have been broadly reviewed.

CuO/ZrO_2 NCs is one of the most prominent member of CuO-based nanostructures which have been widely prepared and applied in the photocatalytic process. The physical and chemical properties of ZrO_2 NPs lead to excellent photodegradation via CuO/ZrO_2 NCs (Guerrero-Araque et al., 2017a; Guerrero-Areque et al., 2017b; Renuka et al., 2017). Nanda et al. (2017) prepared CuO/ZrO_2 –MCM-41 NCs via integrating ZrO_2 into the MCM-41 (M-41) framework, then loading CuO NPs using the wetness impregnation process while maintaining a Si/Zr ratio of 10. For the photoreduction of Cr^{6+}, CuO/ZrO_2–MCM-41 was found to be an effective photocatalyst. Within 30 min, CuO/ZrO_2–MCM-41 NCs achieved at 99% reduction in Cr^{6+} (Babu et al., 2020). CuO/ZrO_2 NCs were prepared via modified sol-gel and solid-state process. The structural and morphological properties of as-prepared samples were compared. Then, The photocatalytic H_2 evolution from oxalic acid solution under solar irradiation was used to examine the photocatalytic activity of CuO/ZrO_2 NCs. It was reported that when

CuO/ZrO_2 NCs photocatalyst is made by sol-gel process and the mole ratio of CuO to ZrO_2 is 40%, the optimum activity of photocatalytic H_2 evolution (2.41 mmol/h.µ) is achieved (Kumar et al., 2020).

In this study, CuO/ZrO_2 NCs as a photocatalys was examined during photocatalytic degradation process in the efficient removal of Sulfamonomethoxine (SMM) from pharmaceutical industry wastewater plant, İzmir, Turkey. Different pH values (3.0, 4.0, 7.0, 9.0, 10.0 and 12.0), increasing SMM concentrations (5 mg/l, 10 mg/l, 20 mg/l and 40 mg/l), increasing CuO/ZrO_2 NCs concentrations (100 mg/l, 200 mg/l, 400 mg/l, 800 mg/l and 1000 mg/l), different CuO/ZrO_2 NCs mass ratios (1/2, 2/3, 3/4, 4/4, 4/3, 3/2, 2/1), increasing recycle times (1., 2., 3., 4., 5., 6. and 7.) was operated during photocatalytic degradation process in the efficient removal of SMM in pharmaceutical industry wastewater. The characteristics of the synthesized NPs were assessed using XRD, DRS, FESEM, EDX, FTIR, TEM and XPS analyses, respectively. The acute toxicity assays were operated with Microtox (*Aliivibrio fischeri*) and *Daphnia magna* acute toxicity tests. The photocatalytic degradation mechanisms of CuO/ZrO_2 NCs and the reaction kinetics of SMM were evaluated in pharmaceutical industry wastewater during photocatalytic degradation process. Cost analysis was evaluated for SMM removal with CuO/ZrO_2 NCs by photocatalytic degradation process in pharmaceutical industry wastewater. ANOVA statistical analysis was used for all experimental samples.

2. MATERIALS AND METHODS

2.1. Characterization of Pharmaceutical Industry Wastewater

Characterization of the biological aerobic activated sludge proses from a pharmaceutical industry wastewater plant, İzmir, Turkey was performed. The results are given as the mean value of triplicate samplings **(Table 1).**

Table 1: Characterization of Pharmaceutical Industry Wastewater

Parameters	**Unit**	**Concentrations**
Chemical oxygen demand-total (COD_{total})	(mg/l)	4000
Chemical oxygen demand-dissolved ($COD_{dissolved}$)	(mg/l)	3200
Biological oxygen demand-5 days (BOD_5)	(mg/l)	1500
BOD_5 / $COD_{dissolved}$		0.5
Total organic carbons (TOC)	(mg/l)	1800
Dissolved organic carbons (DOC)	(mg/l)	1100
pH		8.3
Salinity as Electrical conductivity (EC)	(mS/cm)	1552
Total alkalinity as $CaCO_3$	(mg/l)	750
Total volatile acids (TVA)	(mg/l)	380
Turbidity (Nephelometric Turbidity unit, NTU)	NTU	7.2
Color	1/m	50
Total suspended solids (TSS)	(mg/l)	250
Volatile suspended solids (VSS)	(mg/l)	187
Total dissolved solids (TDS)	(mg/l)	825
Nitride (NO_2^-)	(mg/l)	1.7
Nitrate (NO_3^-)	(mg/l)	1.91
Ammonium (NH_4^+)	(mg/l)	2.3
Total Nitrogen (Total-N)	(mg/l)	3.2
Sulfite (SO_3^{-2})	(mg/l)	21.4
Sulfate (SO_4^{-2})	(mg/l)	29.3

Chloride (Cl^-)	(mg/l)	37.4
Bicarbonate (HCO_3^-)	(mg/l)	161
Phosphate (PO_4^{-3})	(mg/l)	16
Total Phosphorus (Total-P)	(mg/l)	40
Total Phenols	(mg/l)	70
Oil & Grease	(mg/l)	220
Cobalt (Co^{+3})	(mg/l)	0.2
Lead (Pb^{+2})	(mg/l)	0.4
Potassium (K^+)	(mg/l)	17
Iron (Fe^{+2})	(mg/l)	0.42
Chromium (Cr^{+2})	(mg/l)	0.44
Mercury (Hg^{+2})	(mg/l)	0.35
Zinc (Zn^{+2})	(mg/l)	0.11

2.2. Preparation of CuO NPs

CuO NPs were prepared as the following: First, copper sulfate ($CuSO_4$) and ammonia (NH_3) were applied as reactants. The stock solution of 0.1 M $CuSO_4$ was prepared in 100 ml deionized water. To this stock solution, aqueous NH_3 was added under continuous stirring to get the reactants at pH=9.0. The solution is next transferred into Teflon lined sealed stainless steel autoclaves and maintained at a constant temperature of 200^{o}C for 6 h. It was then let to cool to 35 ℃. The precipitate so obtained is placed in a furnace and calcined for 2 h at 500^{o}C.

2.3. Synthesis of ZrO_2 NPs

In a conventional synthesis, in 100 ml of distilled water 0.1 M $ZrOCl_2.8H_2O$ was dissolved with effective stirring. After a few minutes, 0.2 M of KOH is added to the above solution. Afterward, the solution formed is transferred into a stainless steel Teflon lined sterilized capacity of 100 ml and kept in an oven at 180^{o}C for 16 h. To remove the soluble impurities and depress agglomeration, the resulting precipitates are cleaned with distilled water and absolute ethanol (C_2H_6O). The final product was dried for 3 h in a vacuum at 80^{o}C.

2.4. Preparation of CuO/ZrO_2 NCs

The as-prepared CuO and ZrO_2 nanostructures were dispersed in deionized water under vigorous stirring separately. After that, the CuO NPs dispersion was added to ZrO_2 NPs dispersion under ultrasonic for 60 min at 25^{o}C room temperature. The final CuO/ZrO_2 NCs was filtered and dried at 60^{o}C for 10 h.

2.5. Photocatalytic Degradation Experiments

The photocatalytic activity of CuO/ZrO_2 NCs was studied against the photodegradation of SMM antibiotic under ultraviolet (UV) and visible irradiation. To attain the adsorption–desorption equilibrium, 0.03 of CuO/ZrO_2 NCs powder was dispersed into a 50 ml solution of SMM with the concentration of 1 mg/l, then stirred in the dark for 30 min. After then, the as-obtained suspension was exposed to the light of various wavelengths. For providing UV-Vis test, 5 ml suspensions were taken at various periods and filtered to remove the CuO/ZrO_2 NCs.

2.6. Photocatalytic Degradation Reactor

A 2 liter cylinder quartz glass reactor was used for the photodegradation experiments in the pharmaceutical industry wastewater at different operational conditions. 1000 ml pharmaceutical industry wastewater was filled for experimental studies and the photocatalyst were added to the cylinder quartz glass reactors. The UV-A lamps (light intensity=147

mW/cm^2) were placed to the outside of the photo-reactor with a distance of 3 mm. The photocatalytic reactor was operated with constant stirring (1.5 rpm) during the photocatalytic degradation process. In a typical experiment, 25 mg of the sample was added to 50 ml of target pollutant solution. Prior to irradiation, the suspensions were stirred in dark for 100 min to reach adsorption/desorption equilibrium. 10 ml of the reacting solution were sampled and centrifugated at 10000 rpm, at different time intervals. The UV irradiation treatments were created using one or three UV-A lamp emitting in the 350–400 nm range (λ_{max}=368 nm; FWHM=17 nm; Actinic BL TL-D 18W, Philips). Seven 50 W UV-A lamps (Total: 350 W UV-A lamps) were used during experimental conditions for this study. The residual concentration of organic solution in the filtrate was analyzed by using UV–vis spectrophotometer.

2.7. Characterization

2.7.1. X-Ray Diffraction Analysis

Powder XRD patterns were recorded on a Shimadzu XRD-7000, Japan diffractometer using Cu Kα radiation (λ = 1.5418 Å, 40 kV, 40 mA) at a scanning speed of 1^o /min in the 10-80^o 2θ range. Raman spectrum was collected with a Horiba Jobin Yvon-Labram HR UV-Visible NIR (200-1600 nm) Raman microscope spectrometer, using a laser with the wavelength of 512 nm. The spectrum was collected from 10 scans at a resolution of 2 /cm. The zeta potential was measured with a SurPASS Electrokinetic Analyzer (Austria) with a clamping cell at 300 mbar.

2.7.2. Field Emission Scanning Electron Microscopy (FESEM) Analysis

The morphological features and structure of the synthesized catalyst were investigated by a FESEM (FESEM, Hitachi S-4700), equipped with an EDX spectrometry device (TESCAN Co., Model III MIRA) to investigate the composition of the elements present in the synthesized catalyst.

2.7.3. Energy Dispersive X-Ray (EDX) Spectroscopy Analysis

The morphological features and structure of the synthesized catalyst were researhed by an EDX spectrometry device (TESCAN Co., Model III MIRA) to investigate the composition of the elements present in the synthesized catalyst.

2.7.4. Fourier Transform Infrared Spectroscopy (FTIR) Analysis

The FTIR spectra of samples was recorded using the FT-NIR spectroscope (RAYLEIGH, WQF-510).

2.7.5. Transmission Electron Microscopy (TEM) Analysis

The structure of the samples were analysed TEM analysis. TEM analysis was recorded in a JEOL JEM 2100F, Japan under 200 kV accelerating voltage. Samples were prepared by applying one drop of the suspended material in ethanol onto a carbon-coated copper TEM grid, and allowing them to dry at 25^oC room temperature.

2.7.6. Diffuse Reflectance UV-Vis Spectra (DRS) Analysis

DRS Analysis in the range of 200–800 nm were recorded on a Cary 5000 UV-Vis Spectrophotometer from Varian. DRS was used to monitor the OFX antibiotic concentration in experimental samples.

2.7.7. X-Ray Photoelectron Spectroscopy (XPS) Analysis

The valence state of the biogenic palladium nanoparticles was investigated and was analyzed using XPS (ESCALAB 250Xi, England). XPS used an Al Kα source and surface chemical composition and reduction state analyses was done, with the core levels recorded using a pass energy of 30 eV (resolution approximately 0.10 eV). The peak fitting of the individual core-levels was done using XPS-peak 41 software, achieving better fitting and component identification. All binding energies were calibrated to the C 1s peak originating from C–H or C–C groups at 284.6 eV.

2.8. Analytical Procedures

Chemical oxygen demand-total (COD_{total}), chemical oxygen demand-dissolved ($COD_{dissolved}$), total phosphorus (Total-P), phosphate phosphorus (PO_4^{-3}-P), total nitrogen (Total-N), ammonium nitrogen (NH_4^+-N), nitrate nitrogen (NO_3^--N), nitrite nitrogen (NO_2^--N), biological oxygen demand 5-days (BOD_5), pH, Temperature [(^oC)], total suspended solids (TSS), total volatile suspended solids (TVSS), total organic carbon (TOC), Oil, Chloride (Cl^-), total phenol, total volatile acids (TVA), disolved organic carbon (DOC), total alkalinity, turbidity, total dissolved solid (TDS), color, sulfide (SO_3^{-2}), sulfate (SO_4^{-2}), bicarbonate (HCO_3^-), salinity, cobalt (Co^{+3}), lead (Pb^{+2}), potassium (K^+), iron (Fe^{+2}), chromium (Cr^{+2}), Mercury (Hg^{+2}) and zinc (Zn^{+2}) were measured according to the Standard Methods (2017) 5220B, 5220D, 4500-P, 4500-PO_4^{-3}, 4500-N, 4500-NH_4^+, 4500-NO_3^-, 4500-NO_2^-, 5210B, 4500-H^+, 2320, 2540D, 2540E, 5310, 5520, 4500-Cl^-, 5530, 5560B, 5310B, 2320, 2130, 2540E, 2120, 4500-SO_3^{-2}, 4500-SO_4^{-2}, 5320, 2520, 3500-Co^{+3}, 3500-Pb^{+2}, 3500- K^+, 3500-Fe^{+2}, 3500-Cr^{+2}, 3500- Hg^{+2}, 3500-Zn^{+2}, respectively (Lipps et al., 2022).

Total-N, NH_4^+-N, NO_3^--N, NO_2^--N, Total-P, PO_4^{-3}-P, total phenol, Co^{+3}, Pb^{+2}, K^+, Fe^{+2}, Cr^{+2}, Hg^{+2}, Zn^{+2}, SO_3^{-2}, and SO_4^{-2} were measured with cell test spectroquant kits (Merck, Germany) at a spectroquant NOVA 60 (Merck, Germany) spectrophotometer (2003).

The measurement of color was carried out following the methods described by Olthof and Eckenfelder (1976) and Eckenfelder (1989). According these methods, the color content was determined by measuring the absorbance at three wavelengths (445 nm, 540 nm and 660 nm), and taking the sum of the absorbances at these wavelengths. In order to identify the color in pharmaceutical industry wastewater (25 ml) was acidified at pH=2.0 with a few drops of 6 N HCl and extracted three times with 25 ml of ethyl acetate. The pooled organic phases were dehydrated on sodium sulphate, filtered and dried under vacuum. The residue was sylilated with bis(trimethylsylil)trifluoroacetamide (BSTFA) in dimethylformamide and analyzed by gas chromatography–mass spectrometry (GC-MS) and gas chromatograph (GC) (Agilent Technology model 6890N) equipped with a mass selective detector (Agilent 5973 inert MSD). Mass spectra were recorded using a VGTS 250 spectrometer equipped with a capillary SE 52 column (HP5-MS 30 m, 0.25 mm ID, 0.25 µm) at 220°C with an isothermal program for 10 min. The initial oven temperature was kept at 50^{o}C for 1 min, then raised to 220^{o}C at 25^{o}C/min and from 200 to 300^{o}C at 8^{o}C/min, and was then maintained for 5.5 min. High purity He (g) was used as the carrier gas at constant flow mode (1.5 ml/min, 45 cm/s linear velocity).

The total phenol was monitored as follows: 40 ml of pharmaceutical industry wastewater was acidified to pH=2.0 by the addition of concentrated HCl. Total phenol was then extracted with ethyl acetate. The organic phase was concentrated at 40°C to about 1 ml and silylized by the addition of N,O-bis(trimethylsilyl) acetamide (BSA). The resulting trimethylsilyl derivatives were analysed by GC-MS (Hewlett-Packard 6980/HP5973MSD).

Methyl tertiary butyl ether (MTBE) was used to extract oil from the water and NPs. GC-MS analysis was performed on an Agilent gas chromatography (GC) system. Oil concentration was measured using a UV–vis spectroscopy fluorescence spectroscopy and a GC–MS (Hewlett-Packard 6980/HP5973MSD). UV–vis absorbance was measured on a UV–

vis spectrophotometer and oil concentration was calculated using a calibration plot which was obtained with known oil concentration samples.

2.9. Acute Toxicity Assays

2.9.1. Microtox Acute Toxicity Test

Toxicity to the bioluminescent organism *Aliivibrio fischeri (*also called *Vibrio fischeri* or *V. fischeri*) was assayed using the Microtox measuring system according to DIN 38412L34, L341, (EPS 1/ RM/24 1992). Microtox testing was performed according to the standard procedure recommended by the manufacturer (Lange, 1994). A specific strain of the marine bacterium, *V. fischeri*-Microtox LCK 491 kit (Lange, 1994) was used for the Microtox acute toxicity assay. Dr. LANGE LUMIX-mini type luminometer was used for the microtox toxicity assay (Lange, 2010).

2.9.2. *Daphnia magna* Acute Toxicity Test

To test toxicity, 24-h born *Daphnia magna* were used as described in Standard Methods sections 8711A, 8711B, 8711C, 8711D and 8711E, respectively (Lange, 1996). After preparing the test solution, experiments were carried out using 5 or 10 *Daphnia magna* introduced into the test vessels. These vessels had 100 ml of effective volume at 7.0– 8.0 pH, providing a minimum dissolved oxygen (DO) concentration of 6 mg/l at an ambient temperature of 20–25°C. Young *Daphnia magna* were used in the test (≤24 h old); 24–48 h exposure is generally accepted as standard for a *Daphnia magna* acute toxicity test. The results were expressed as mortality percentage of the *Daphnia magna*. Immobile animals were reported as dead *Daphnia magna*.

2.10. Statistical Analysis

ANOVA analysis of variance between experimental data was performed to detect F and *P* values. The ANOVA test was used to test the differences between dependent and independent groups, (Zar, 1984). Comparison between the actual variation of the experimental data averages and standard deviation is expressed in terms of F ratio. F is equal (found variation of the date averages/expected variation of the date averages). *P* reports the significance level, and d.f indicates the number of degrees of freedom. Regression analysis was applied to the experimental data in order to determine the regression coefficient R^2, (Statgraphics Centurion XV, 2005). The aforementioned test was performed using Microsoft Excel Program.

All experiments were carried out three times and the results are given as the means of triplicate samplings. The data relevant to the individual pollutant parameters are given as the mean with standard deviation (SD) values.

3. RESULTS AND DISCUSSIONS

3.1. Characterizations of CuO/ZrO_2 NCs

3.1.1. The Results of X-Ray Diffraction (XRD) Analysis

The results of XRD analysis was observed to pure CuO NPs and pure ZrO_2 NPs, respectively, in pharmaceutical industry wastewater with photocatalytic degradation process for SMM antibiotic removal **(Figure 1).** The characterization peaks were observed at 2θ values of 30.05^o, 33.19^o, 37.18^o, 39.75^o, 48.11^o, 59.07^o, 62.58^o, 67.80^o and 75.12°, respectively, corresponding to the (110), (002), (111), (202), (020), (202), (113), (311) and (220) planes of implying pure CuO NPs in pharmaceutical industry wastewater with photocatalytic degradation process for SMM antibiotic removal **(Figure 1a)**. The characterization peaks were obtained at 2θ values of 30.04o, 32.79o, 43.52o, 50.59o, 59.17o, 61.78o 65.24o and 74.37o, respectively, corresponding to the (110), (011), (110), (111),

(002), (200), (211) and (220) planes of implying pure ZrO_2 NPs in pharmaceutical industry wastewater with photocatalytic degradation process for SMM antibiotic removal **(Figure 1b)**.

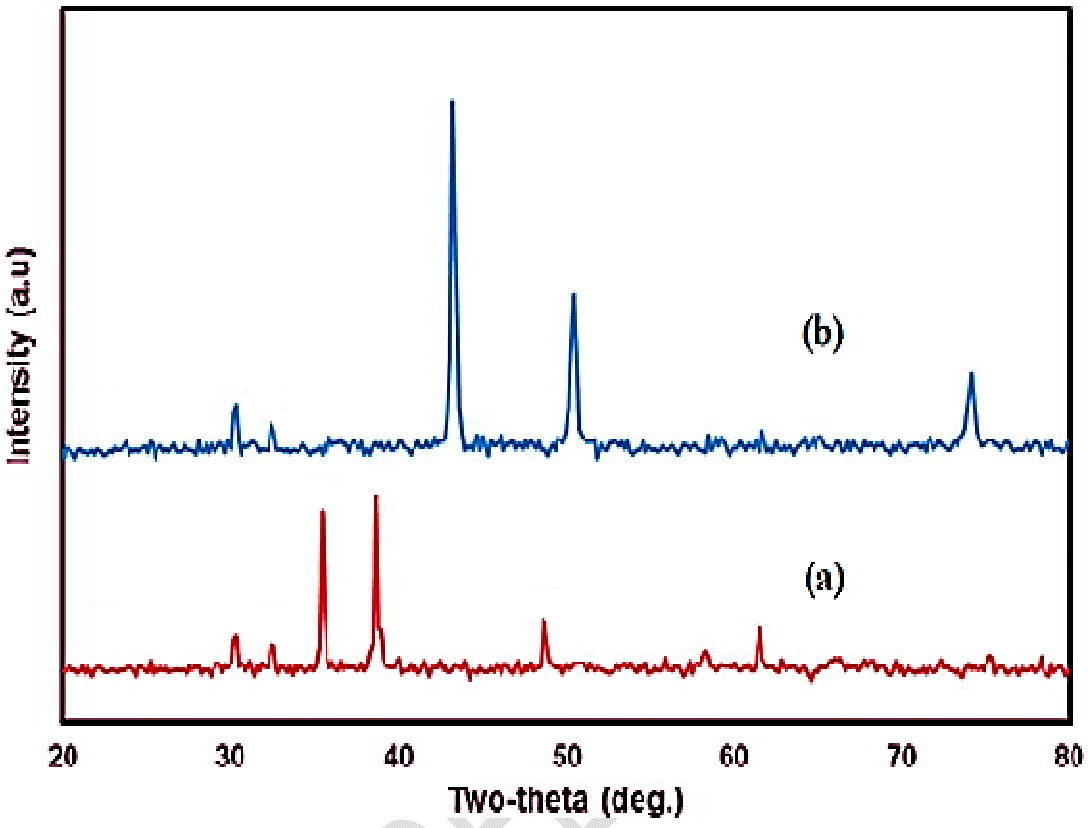

Figure 1: The XRD patterns of **(a)** pure CuO NPs (red pattern) and **(b)** pure ZrO_2 NPs (blue pattern), respectively, in pharmaceutical industry wastewater with photocatalytic degradation process for SMM antibiotic removal.

3.1.2. The Results of Diffuse reflectance UV-Vis Spectra (DRS) Analysis

The absorption spectra of SMM was observed in DRS Analysis (**Figure 2**). First, the absorption spectra of SMM were obtained at a maximum concentration of 1600 mg/l in the wavelength range from 200 nm to 600 nm using diffuse reflectance UV-Vis spectra **(Figure 2).** Absorption peaks were observed at wavelength of 225 nm for CuO/ZrO2 NCs, respectively, in pharmaceutical industry wastewater with photocatalytic degradation process for SMM antibiotic removal **(Figure 2).**

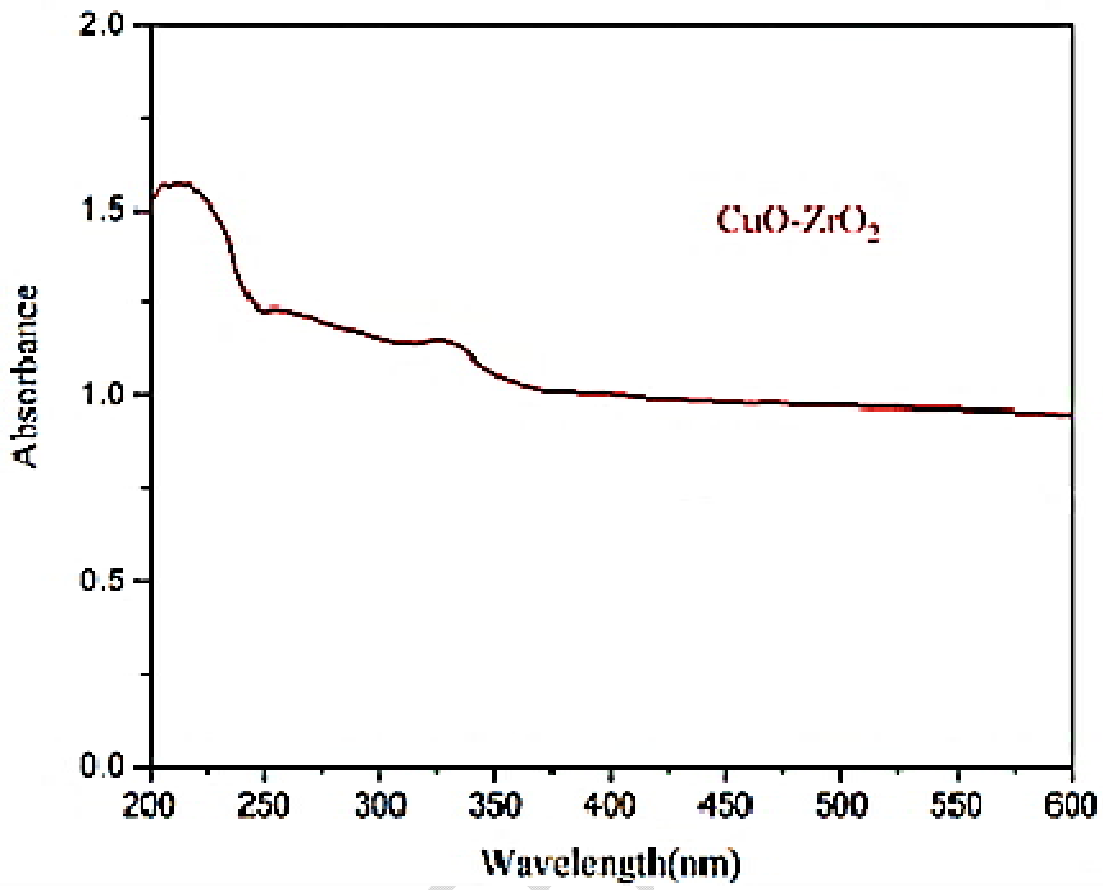

Figure 2: The DRS patterns of CuO/ZrO_2 NCs in pharmaceutical industry wastewater with photocatalytic degradation process for SMM antibiotic removal.

3.1.3. The Results of Field Emission Scanning Electron Microscopy (FESEM) Analysis

The morphological features of pure CuO NPs, pure ZrO_2 NPs and CuO/ZrO_2 NCs were characterized through FESEM images (**Figure 3**). The FESEM images of pure CuO NPs were obtained in in pharmaceutical industry wastewater with photocatalytic degradation process for SMM antibiotic removal (**Figure 3a**). The FESEM images of pure ZrO_2 NPs were observed in pharmaceutical industry wastewater with photocatalytic degradation process for SMM antibiotic removal (**Figure 3b**). The FESEM images of CuO/ZrO_2 NCs were characterized in pharmaceutical industry wastewater with photocatalytic degradation process for SMM antibiotic removal (**Figure 3c**).

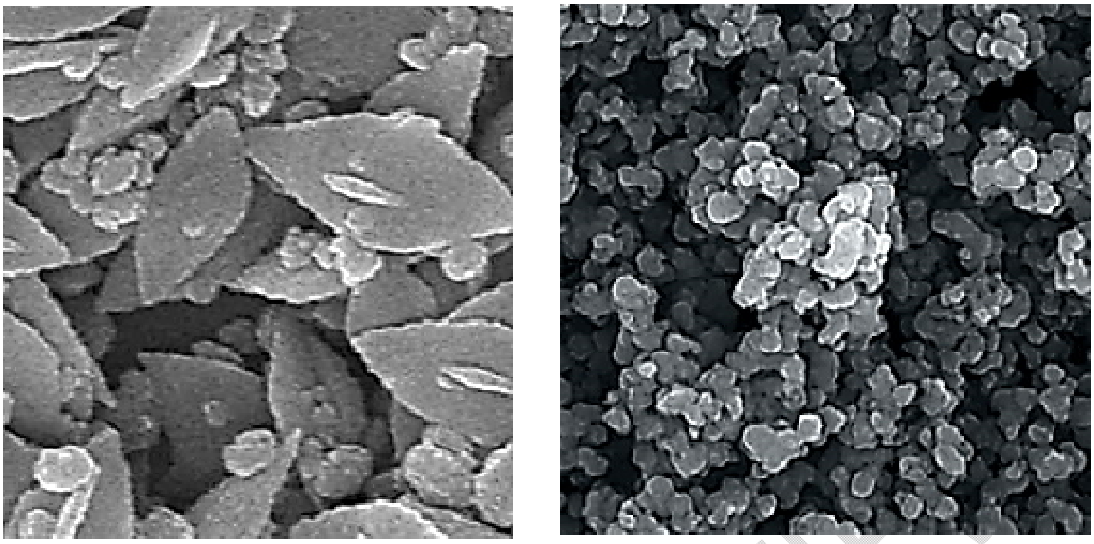

(a) **(b)**

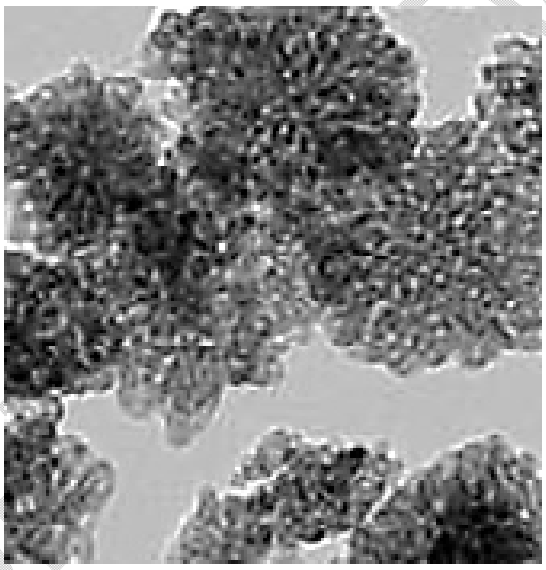

(c)

Figure 3: FESEM images of **(a)** pure CuO NPs, **(b)** pure ZrO_2 NPs and **(c)** CuO/ZrO_2 NCs, respectively, in pharmaceutical industry wastewater with photocatalytic degradation process for SMM antibiotic removal.

3.1.4. The Results of Energy Dispersive X-Ray (EDX) Spectroscopy Analysis

The EDX analysis was also performed to investigate the composition of CuO/ZrO_2 NCs in pharmaceutical industry wastewater with photocatalytic degradation process for SMM antibiotic removal (**Figure 4**).

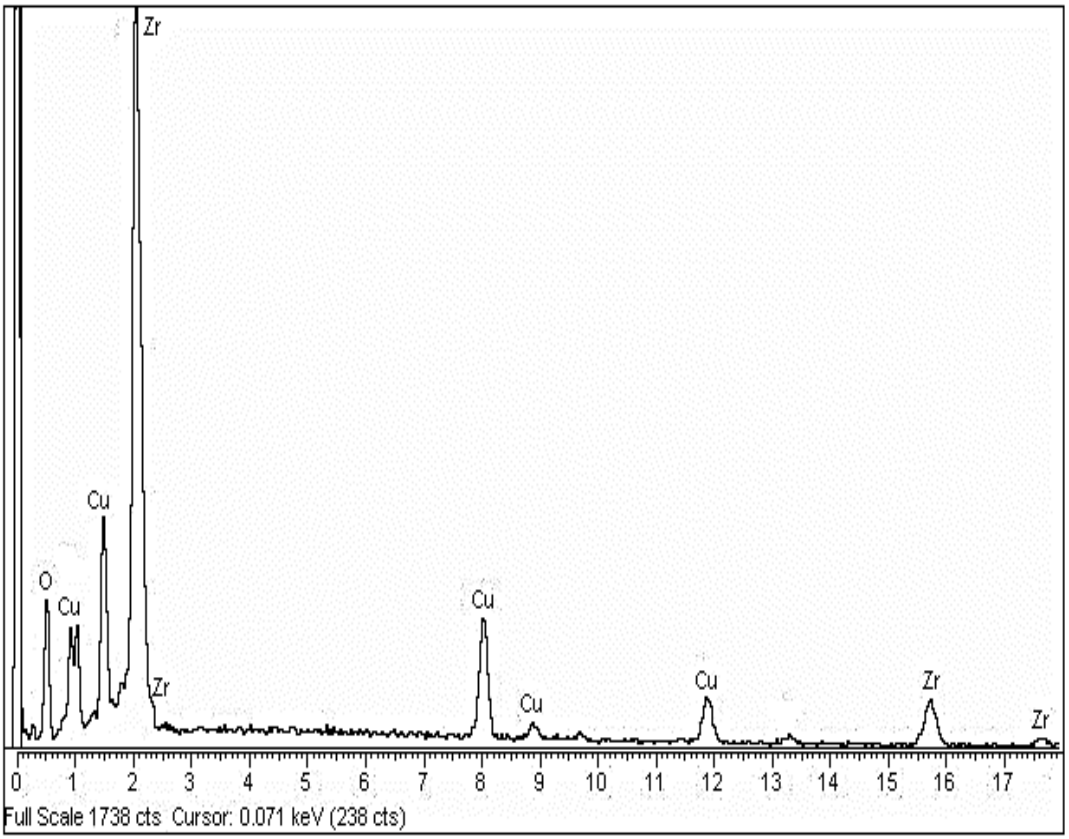

Figure 4: EDX spectrum of CuO/ZrO_2 NCs, respectively, in pharmaceutical industry wastewater with photocatalytic degradation process for SMM antibiotic removal.

3.1.5. The Results of Fourier Transform Infrared Spectroscopy (FTIR) Analysis

The FTIR spectrum of CuO/ZrO_2 NCs in pharmaceutical industry wastewater with photocatalytic degradation process for SMM antibiotic removal **(Figure 5)**. The main peaks of FTIR spectrum for CuO/ZrO_2 NCs was observed at 3475 cm^{-1}, 1051 cm^{-1}, 627 cm^{-1} and 512 cm^{-1} wavenumber, respectively (**Figure 5**).

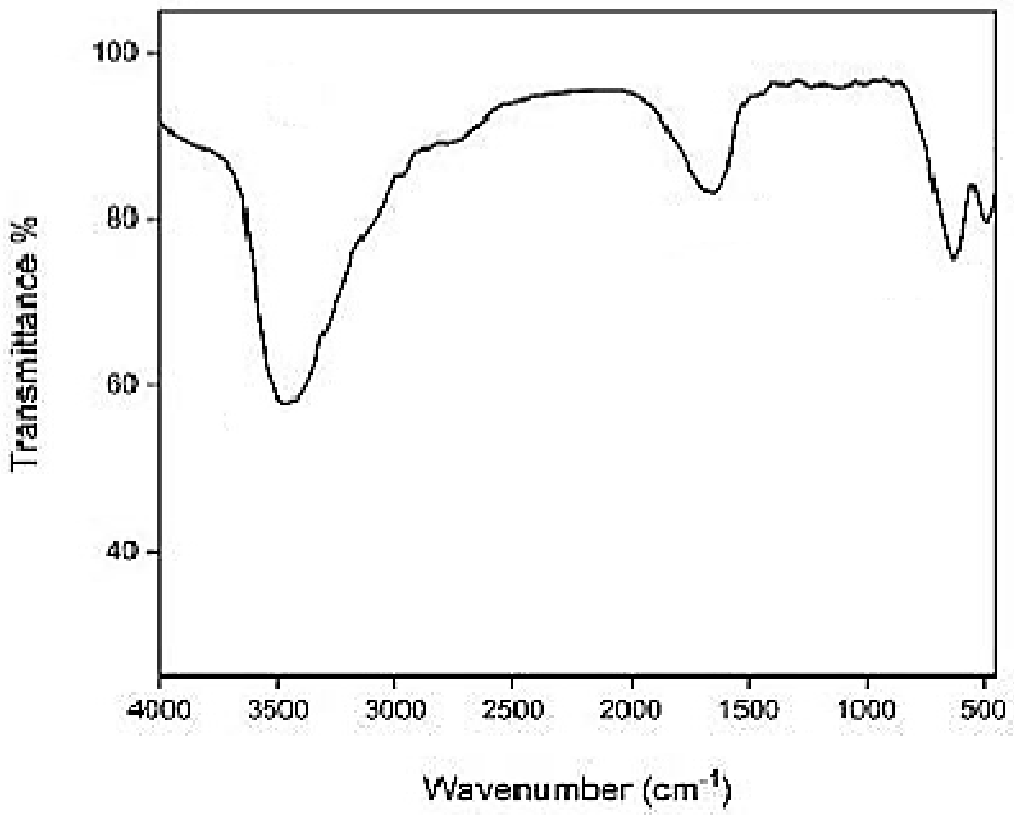

Figure 5: FTIR spectrum of CuO/ZrO_2 NCs in pharmaceutical industry wastewater with photocatalytic degradation process for SMM antibiotic removal.

3.1.6. The Results of Transmission Electron Microscopy (TEM) Analysis

The TEM images of CuO/ZrO_2 NCs was observed in micromorphological structure level in pharmaceutical industry wastewater with photocatalytic degradation process for SMM antibiotic removal (**Figure 6).**

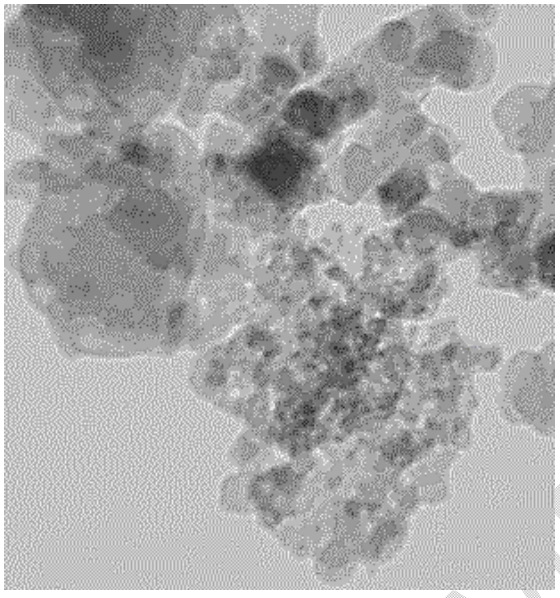

Figure 6: TEM images of CuO/ZrO_2 NCs in micromorphological structure level in pharmaceutical industry wastewater with photocatalytic degradation process for SMM antibiotic removal.

3.1.7. X-Ray Photoelectron Spectroscopy (XPS) Analysis

The XPS analysis of CuO/ZrO_2 NCs in micromorphological structure level in pharmaceutical industry wastewater with photocatalytic degradation process for SMM antibiotic removal (**Figure 7**).

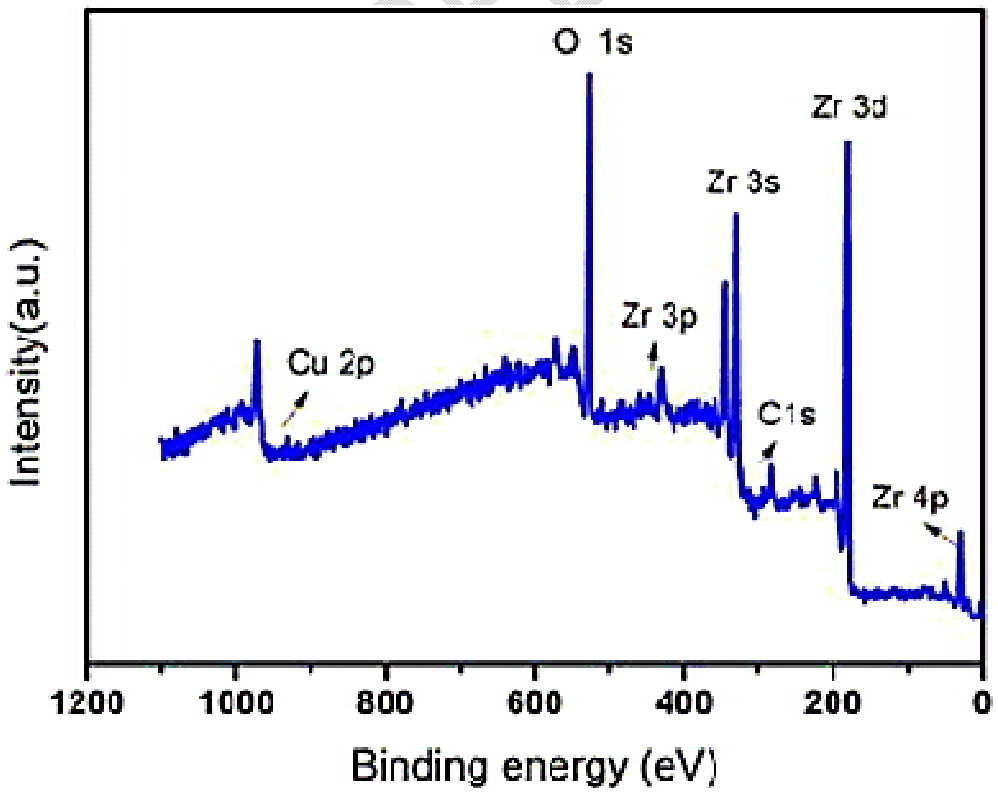

Figure 7: XPS spectra of CuO/ZrO_2 NCs in micromorphological structure level in pharmaceutical industry wastewater with photocatalytic degradation process for SMM antibiotic removal.

3.2. The Reaction Kinetics of SMM Antibiotic

The reaction kinetics SMM were investigated using the Langmuir–Hinshelwood first-order kinetic model, expressed by Eddy et al. (2015), as following **Equation (1):**

$$r_o = -\frac{dC}{dt} = kC \quad (1)$$

where; r_o: denotes the initial photocatalytic degradation reaction rate (mg/l.min), and k: denotes the rate constant of a first-order reaction. At the beginning of the reaction, t = 0, $C_t = C_0$, the equation can be obtained after integration as following **Equation (2):**

$$ln\frac{C}{C_0} = -kt \quad (2)$$

where; C_0 and C : are the initial and final concentration (mg/l) of SMM; the solution at t (min) and k (1/min) are the rate constant.

The correlation coefficients had R^2 values greater than 0.9, as a result, the first-order kinetic model fit the experimental data well. The first-order rate constants (k) were determined from the slope of the linear plots.

3.3. Photocatalytic Degradation Mechanisms

The photocatalytic performance of the catalyst in the degradation of SMM is determined by photons. The degradation mechanism of SMM by hydroxyl radicals ($OH^{\bullet}$) radicals concerning CuO/ZrO_2 NCs as following equations (**Equation 3, Equation 4, Equation 5, Equation 6, Equation 7, Equation 8, Equation 9** and **Equation 10**):

$$CuO/ZrO_2 + hv \rightarrow CuO\ (h^+ + e^-)/ZrO_2\ (h^+ + e^-) \quad (3)$$

$$CuO\ (h^+ + e^-)/ZrO_2\ (h^+ + e^-) \rightarrow CuO\ (h^+ + h^+)/ZrO_2\ (e^- + e^-) \quad (4)$$

$$e^- + O_2 \rightarrow O_2^- \quad (5)$$

$$h^+ + H_2O \rightarrow OH + h^+ \quad (6)$$

$$ZrO_2(h^+) + H_2O \rightarrow OH + H^+ + ZrO_2 \quad (7)$$

$$OH^- + ZrO_2(h^+) \rightarrow OH + ZrO_2 \quad (8)$$

$$O_2 + e^- \rightarrow O_2^-$$
(9)

$$SMM + O_2^- \ /OH \ \rightarrow CO_2 + H_2O + Degradation\ Products$$
(10)

CuO/ZrO_2 NCs absorbs photons with energies greater than the photocatalyst bandgap. As a result, the electron in the VB jumps to the CB, leaving a hole in the CB. The electrons present in the CB and VB will react with O_2 and H_2O molecules which are absorbed by the photocatalyst and lead to the formation of $OH^\bullet$ radicals which react with SMM. $OH^\bullet$ radicals are produced when the photocatalyst surface is illuminated with photons, and $OH^\bullet$ radicals are strong oxidising species, with an oxidation potential of approximately 2.8 V [as opposed to Normal hydrogen electrode (NHE)], which may increase total pollutant mineralisation. Normally, the higher the rate of formation of $OH^\bullet$ radicals, the greater the separation efficiency of electron-hole pairs. In this way, there is a correlation between the increased photocatalytic activity and the rate of formation of $OH^\bullet$ radicals. The $OH^\bullet$ radicals generation of CuO/ZrO_2 NCs was extremely high, indicating that the sample has a high electron and hole separation rate.

3.4. Effect of Increasing pH values for SMM Removal in Pharmaceutical Industry Wastewater during Photocatalytic Degradation Process

Increasing pH values (pH=3.0, pH=4.0, pH=7.0, pH=9.0, pH=10.0 and pH=12.0, respectively) was examined during photocatalytic degradation process in pharmaceutical industry wastewater for SMM removal, at 350 W UV-vis light irradiation power, at 147 mW/cm^2 light intensity, after 120 min photocatalytic degradation time and at 25^oC, respectively (**Figure 8).** 52.2%, 75.7%, 80.4%, 87.5% and 95.8% SMM removal efficiencies was measured at pH=3.0, pH=4.0, pH=7.0, pH=9.0 and pH=10.0, respectively, at 350 W UV-vis light irradiation power, at 147 mW/cm^2 light intensity, after 120 min photocatalytic degradation time and at 25^oC, respectively (**Figure 8**). The maximum 99.6% SMM removal efficiency was obtained during photocatalytic degradation process in pharmaceutical industry wastewater, at 350 W UV-vis light irradiation power, at 147 mW/cm^2 light intensity, after 120 min photocatalytic degradation time, at pH=12.0 and at 25^oC, respectively (**Figure 8**).

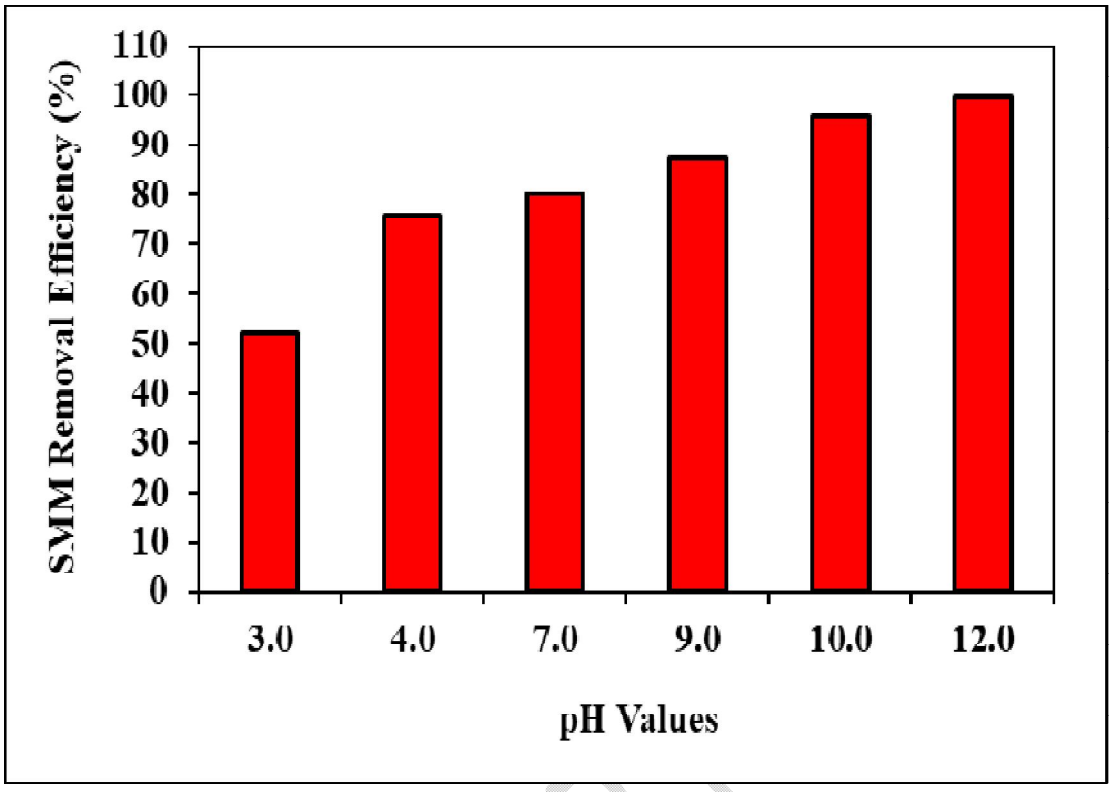

Figure 8: Effect of increasing pH values for SMM removal in pharmaceutical industry wastewater during photocatalytic degradation process, at 350 W UV-vis light irradiation power, at 147 mW/cm^2 light intensity, after 120 min photocatalytic degradation time and at 25^{o}C, respectively.

3.5. Effect of Increasing SMM Concentrations for SMM Removal in Pharmaceutical Industry Wastewater during Photocatalytic Degradation Process

Increasing SMM concentrations (5 mg/l, 10 mg/l, 20 mg/l and 40 mg/l) were operated at 350 W UV-vis irradiation power, at 147 mW/cm^2 light intensity, after 120 min photocatalytic degradation time, at pH=12.0 and at 25^{o}C, respectively (**Figure 9**). 90.3%, 82.1% and 59.7% SMM removal efficiencies were obtained to 10 mg/l, 20 mg/l and 40 mg/l SMM concentrations, at 350 W UV-vis irradiation power, at 147 mW/cm^2 light intensity, after 120 min photocatalytic degradation time, at pH=12.0 and at 25^{o}C, respectively (**Figure 9**). The maximum 99.2% SMM removal efficieny was found with photocatalytic degradation process in pharmaceutical industry wastewater, at 5 mg/l SMM, at 350 W UV-vis irradiation power, at 147 mW/cm^2 light intensity, after 120 min photocatalytic degradation time, at pH=12.0 and at 25^{o}C, respectively (**Figure 9**).

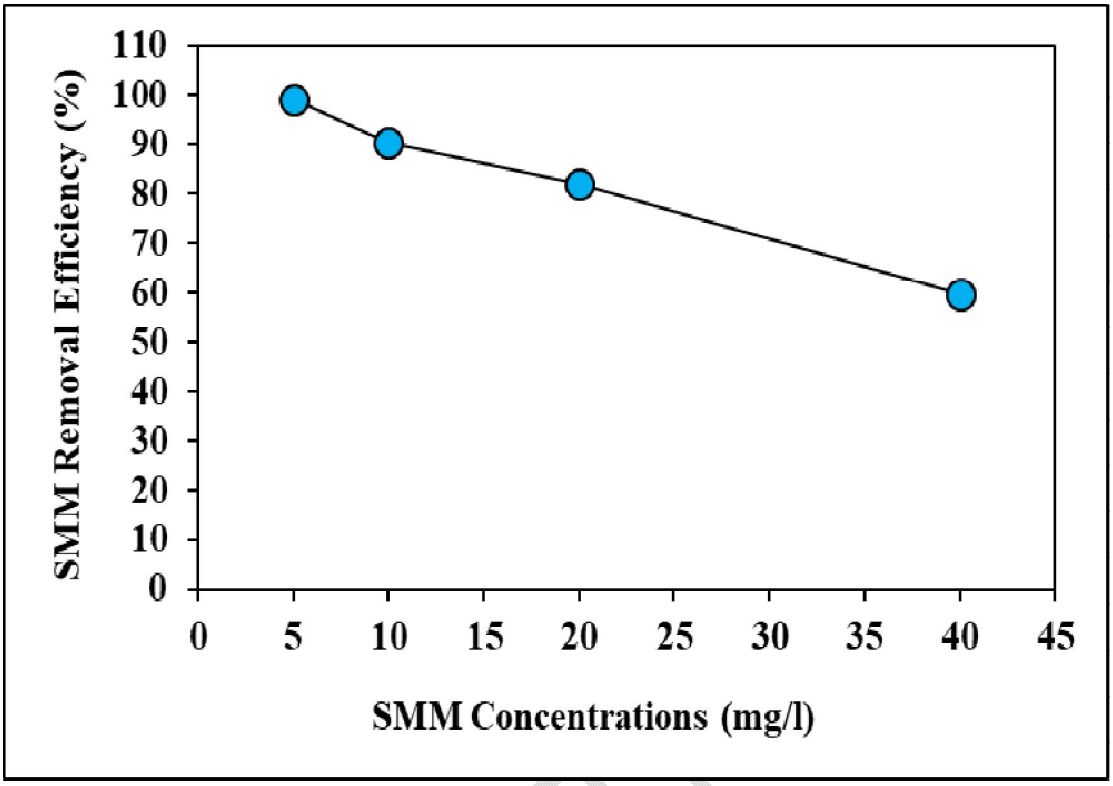

Figure 9: Effect of increasing SMM concentrations for SMM removal in pharmaceutical industry wastewater during photocatalytic degradation process, at 350 W UV-vis irradiation power, at 147 mW/cm^2 light intensity, after 120 min photocatalytic degradation time, at pH=12.0 and at 25^{o}C, respectively.

3.6.Effect of Increasing CuO/ZrO_2 NCs Concentrations for SMM Removals in Pharmaceutical Industry Wastewater during Photocatalytic Degradation Process

Increasing CuO/ZrO_2 NCs concentrations (100 mg/l, 200 mg/l, 400 mg/l, 800 mg/l and 1000 mg/l) were operated at 5 mg/l SMM, at 350 W UV-vis light irradiation power, at 147 mW/cm^2 light intensity, after 120 min photocatalytic degradation time, at pH=12.0 and at 25^{o}C, respectively (**Figure 10**). 60.5%, 70.1%, 78.8% and 80.1% SMM removal efficiencies were obtained to 100 mg/l, 200 mg/l, 400 mg/l and 1000 mg/l CuO/ZrO_2 NCs concentrations, respectively, at 5 mg/l SMM, at 350 W UV-vis light irradiation power, at 147 mW/cm^2 light intensity, after 120 min photocatalytic degradation time, at pH=12.0 and at 25^{o}C, respectively (**Figure 10**). The maximum 99.5% SMM removal efficieny was measured to 800 mg/l CuO/ZrO_2 NCs with photocatalytic degradation process in pharmaceutical industry wastewater, at 5 mg/l SMM, at 350 W UV-vis light irradiation power, at 147 mW/cm^2 light intensity, after 120 min photocatalytic degradation time, at pH=12.0 and at 25^{o}C, respectively (**Figure 10**).

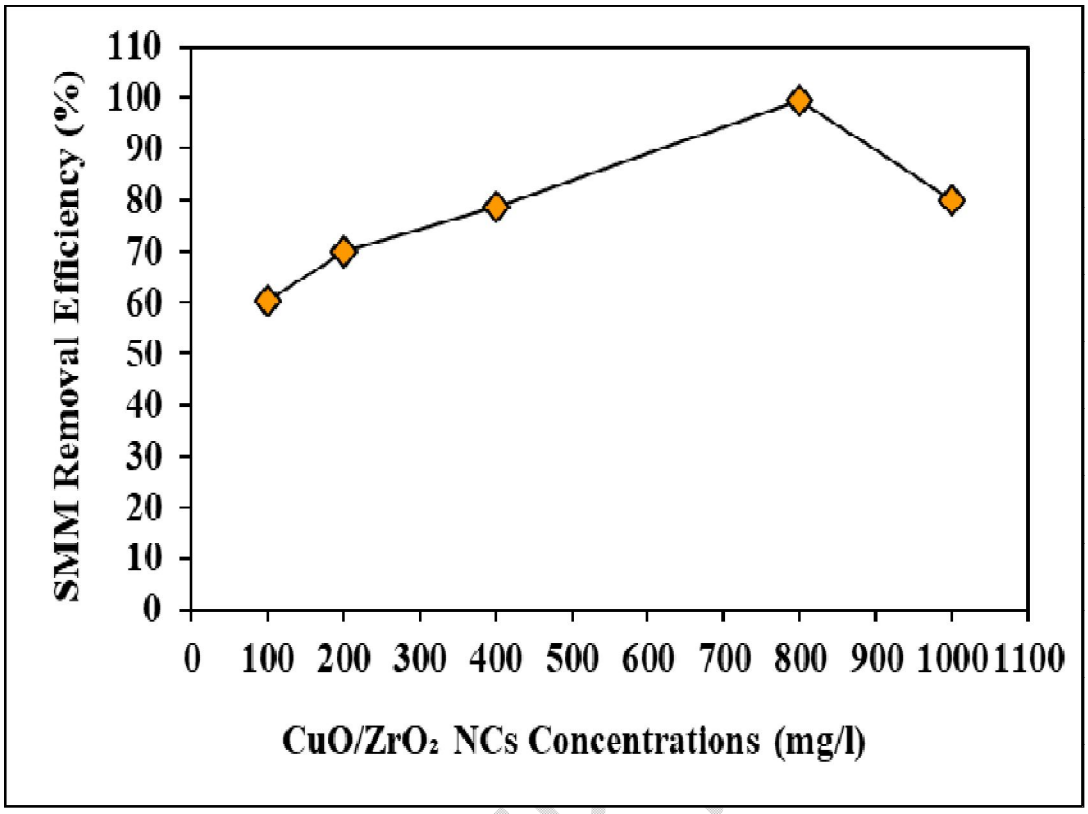

Figure 10: Effect of increasing CuO/ZrO_2 NCs concentrations for SMM removal in pharmaceutical industry wastewater during photocatalytic degradation process, at 5 mg/l SMM, at 350 W UV-vis light irradiation power, at 147 mW/cm^2 light intensity, after 120 min photocatalytic degradation time, at pH=12.0 and at 25^{o}C, respectively.

3.7. Effect of Different CuO/ZrO_2 NCs Mass Ratios for SMM Removals in Pharmaceutical Industry Wastewater during Photocatalytic Degradation Process

Different CuO/ZrO_2 mass ratios (1/2wt, 2/3wt, 3/4wt, 4/4wt, 4/3wt, 3/2 and 2/1wt, respectively) were examined for SMM removal in pharmaceutical industry wastewater during photocatalytic degradation process, at 5 mg/l SMM, at 800 mg/l CuO/ZrO_2 NCs, at 350 W UV-vis light irradiation power, at 147 mW/cm^2 light intensity, after 120 min photocatalytic degradation time, at pH=12.0 and at 25^{o}C, respectively (**Figure 11**). 47.3%, 53.6%, 68.9%, 84.7%, 73.1% and 59.2% SMM removal efficiencies were measured at 1/2wt, 2/3 wt, 3/4wt, 4/4wt, 3/2 and 2/1wt CuO/ZrO_2 NCs mass ratios, respectively, at 5 mg/l SMM, at 800 mg/l CuO/ZrO_2 NCs, at 350 W UV-vis light irradiation power, at 147 mW/cm^2 light intensity, after 120 min photocatalytic degradation time, at pH=12.0 and at 25^{o}C, respectively **(Figure 11**). The maximum 99.4% SMM removal efficiency was measured at 4/3wt CuO/ZrO_2 NCs mass ratios, at 5 mg/l SMM, at 800 mg/l CuO/ZrO_2 NCs, at 350 W UV-vis light irradiation power, at 147 mW/cm^2 light intensity, after 120 min photocatalytic degradation time, at pH=12.0 and at 25^{o}C, respectively **(Figure 11**).

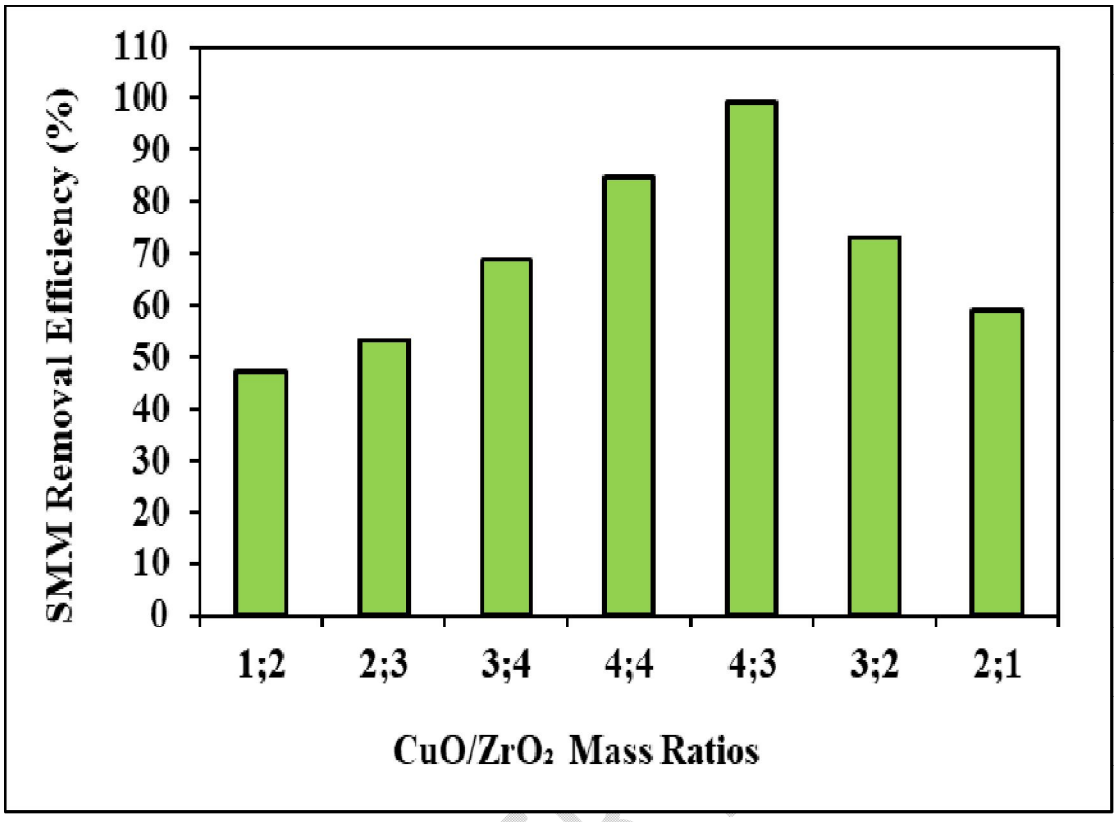

Figure 11: Effect of different CuO/ZrO_2 NCs mass ratios for SMM removal in pharmaceutical industry wastewater during photocatalytic degradation process, at 5 mg/l SMM, at 800 mg/l CuO/ZrO_2 NCs, at 350 W UV-vis light irradiation power, at 147 mW/cm^2 light intensity, after 120 min photocatalytic degradation time, at pH=12.0 and at 25°C, respectively.

3.8. Effect of Different Recycle Times for SMM Removals in Pharmaceutical Industry Wastewater during Photocatalytic Degradation Process

Different recycle times (1., 2., 3., 4., 5., 6. and 7.) were operated for SMM removals in pharmaceutical industry wastewater during photocatalytic degradation process, at 5 mg/l SMM, at 800 mg/l CuO/ZrO_2 NCs, at 4/3wt CuO/ZrO_2 NCs mass rartio, at 350 W UV-vis light irradiation power, at 147 mW/cm^2 light intensity, after 120 min photocatalytic degradation time, at pH=12.0 and at 25°C, respectively (**Figure 12**). 92.6%, 85.2%, 77.8%, 73.2%, 68.6% and 64.1% SMM recovery yields were measured after 2. recycle time, 3. recycle time, 4. recycle time, 5. recycle time, 6. recycle time and 7. recycle time, respectively, at 5 mg/l SMM, at 800 mg/l CuO/ZrO_2 NCs, at 4/3wt CuO/ZrO_2 NCs mass rartio, at 350 W UV-vis light irradiation power, at 147 mW/cm^2 light intensity, after 120 min photocatalytic degradation time, at pH=12.0 and at 25°C, respectively (**Figure 12**). The maximum 99.5% SMM recovery efficiency was measured in pharmaceutical industry wastewater during photocatalytic degradation process, after 1. recycle time, at 5 mg/l SMM, at 800 mg/l CuO/ZrO_2 NCs, at 4/3wt CuO/ZrO_2 NCs mass rartio, at 350 W UV-vis light irradiation power, at 147 mW/cm^2 light intensity, after 120 min photocatalytic degradation time, at pH=12.0 and at 25°C, respectively (**Figure 12**).

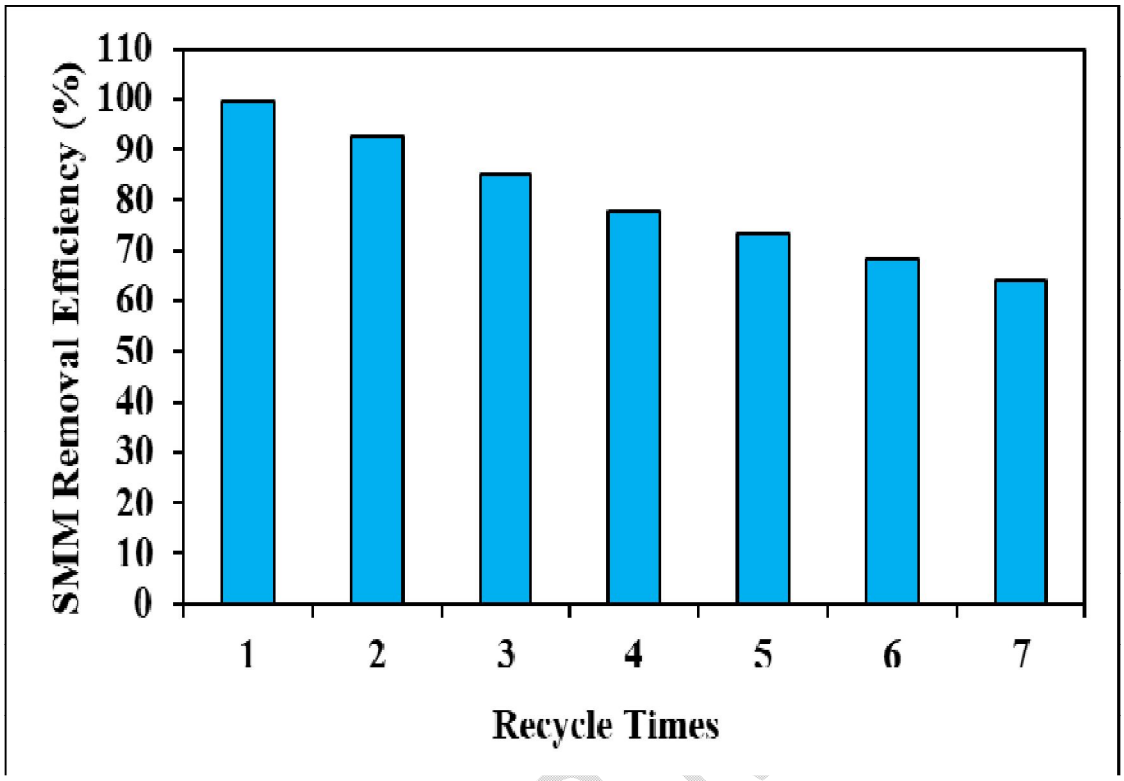

Figure 12: Effect of recycle times for SMM removal in pharmaceutical industry wastewater during photocatalytic degradation process, at 5 mg/l SMM, at 800 mg/l CuO/ZrO_2 NCs, at 4/3wt CuO/ZrO_2 NCs mass rartio, at 350 W UV-vis light irradiation power, at 147 mW/cm^2 light intensity, after 120 min photocatalytic degradation time, at pH=12.0 and at 25°C, respectively.

3.9.Acute Toxicity Assays

3.9.1. Effect of Increasing SMM Concentrations on the Microtox (*Aliivibrio fischeri* or *Vibrio fischeri*) Acute Toxicity Removal Efficiencies in Pharmaceutical Industry Wastewater at Increasing Photocatalytic Degradation Time and Temperature

In Microtox with *Aliivibrio fischeri* (also called *Vibrio fischeri*) acute toxicity test, the initial EC_{90} values at pH=7.0 was found as 825 mg/l at 25°C (**Table 2: SET 1**). After 60 min, 120 min and 180 min photocatalytic degradation time, the EC_{90} values decreased to EC_{57}=414 mg/l to EC_{22}=236 mg/l and to EC_{12}=165 mg/l in SMM=20 mg/l at 30°C (**Table 2: SET 3**). The Microtox (*Aliivibrio fischeri*) acute toxicity removal efficiencies were 41.75%, 80.64% and 91.75% after 60 min, 120 min and 180 min, respectively, in SMM=20 mg/l and at 30°C (**Table 2: SET 3**).

Table 2: Effect of increasing SMM concentrations on Microtox (*Aliivibrio fischeri*) acute toxicity in pharmaceutical industry wastewater after photocatalytic degradation process, at 30°C and at 60°C, respectively.

No	Parameters	Microtox (*Aliivibrio fischeri*) Acute Toxicity Values, * EC (mg/l)			
		25°C			
		0. min	60. min	120. min	180. min
		*EC_{90}	*EC	*EC	*EC

1	Raw ww, control	825		EC_{70}=510		EC_{60}=650		EC_{49}=638	
		30°C				**60°C**			
		0. min	**60. min**	**120. min**	**180. min**	**0. min**	**60. min**	**120. min**	**180. min**
		***EC_{90}**	***EC**	***EC**	***EC**	***EC_{90}**	***EC**	***EC**	***EC**
2	Raw ww, control	825	EC_{70}= 580	EC_{50}= 580	EC_{39}= 548	825	EC_{55}= 550	EC_{40}= 590	EC_{29}= 688
3	SMM=5 mg/l	825	EC_{63}= 421	EC_{28}= 241	EC_{18}= 167	825	EC_{58}= 418	EC_{23}= 265	EC_{13}= 149
	SMM=10 mg/l	825	EC_{62}= 420	EC_{27}= 238	EC_{17}= 166	825	EC_{57}= 413	EC_{22}= 231	EC_{12}= 160
	SMM=20 mg/l	825	EC_{58} =413	EC_{23}= 235	EC_{13}= 164	825	EC_{53}= 549	EC_{18}= 539	EC_{8}= 499
	SMM=40 mg/l	825	EC_{68}= 407	EC_{33}= 229	EC_{23}= 161	825	EC_{63}= 402	EC_{28}= 217	EC_{18}= 147
* EC values were calculated based on COD_{dis} (mg/l).									

The EC_{90} values decreased to EC_{53}, to EC_{18} and to EC_{8} after 60 min, 120 min and 180 min, respectively, in SMM=20 mg/l, at 60°C (**Table 2: SET 3**). The EC_{51}, the EC_{11} and the EC_{7} values were measured as 549 mg/l, 539 mg/l and 499 mg/l, respectively, in SMM=20 mg/l at 60°C. The toxicity removal efficiencies were 47.30%, 86.29% and 97.31% after 60 min, 120 min and 180 min, respectively, in SMM=20 mg/l, at 60°C (**Table 2: SET 3**). 97.31% maximum Microtox (*Aliivibrio fischeri*) acute toxicity removal yield was found in SMM=20 mg/l after 180 min and at 60°C (**Table 2: SET 3**).

The EC_{90} values decreased to EC_{63}=421 mg/l to EC_{28}=241 mg/l and to EC_{18}=167 mg/l after 60 min, 120 min and 180 min, respectively, in SMM=5 mg/l at 30°C (**Table 2: SET 3**). The EC_{90} values decreased to EC_{62}=420 mg/l to EC_{27}=238 mg/l and to EC_{11}=166 mg/l after 60 min, 120 min and 180 min, respectively, in SMM=10 mg/l at 30°C. The EC_{90} values decreased to EC_{68}=407 mg/l to EC_{33}=229 mg/l and to EC_{23}=161 mg/l after 60 min, 120 min and 180 min, respectively, in SMM=40 mg/l at 30°C. The Microtox (*Aliivibrio fischeri* or *Vibrio fischeri)* acute toxicity removals were 86.19%, 86.17% and 80.64% in 5 mg/l, 10 mg/l and 40 mg/l SMM, respectively, after 180 min, at 30°C. It was obtained an inhibition effect of SMM=40 mg/l to *Vibrio fischeri* after 180 min and at 30°C (**Table 2: SET 3**).

The EC_{90} values decreased to EC_{58}=418 mg/l to EC_{23}=265 mg/l and to EC_{13}=149 mg/l after 60 min, 120 min and 180 min, respectively, in SMM=5 mg/l at 60°C (**Table 2: SET 3**). The EC_{90} values decreased to EC_{57}=413 mg/l to EC_{22}=231 mg/l and to EC_{12}=160 mg/l after 60 min, 120 and 180 min, respectively, in SMM=10 mg/l at 60°C. The EC_{90} values decreased to EC_{63}=402 mg/l to EC_{28}=217 mg/l and to EC_{18}=147 mg/l after 60 min, 120 and 180 min, respectively, in SMM=40 mg/l at 60°C. The Microtox (*Aliivibrio fischeri* or *Vibrio fischeri*) acute toxicity removals were 91.75%, 91.72% and 86.21% in 5 mg/l, 10 mg/l and 40 mg/l SMM, respectively, after 180 min, at 60°C. It was observed an inhibition effect of SMM=40 mg/l to Microtox with *Vibrio fischeri* after 180 min, and at 60°C (**Table 2: SET 3**).

3.9.2. Effect of Increasing SMM Concentrations on the *Daphnia magna* Acute Toxicity Removal Efficiencies in Pharmaceutical Industry Wastewater at Increasing Photocatalytic Degradation Time and Temperature

The initial EC_{50} values were observed as 850 mg/l at 25°C (**Table 3: SET 1**). After 60 min, 120 and 180 min photocatalytic degradation time, the EC_{50} values decreased to EC_{32}=349 mg/l to EC_{18}=239 mg/l and to EC_{13}=89 mg/l in SMM=20 mg/l, at 30°C (**Table 3: SET 3**). The toxicity removal efficiencies were 43.85%, 73.76% and 83.54% after 60 min, 120 min and 180 min, respectively, in SMM=20 mg/l at 30°C (**Table 3: SET 3**).

Table 3: Effect of increasing SMM concentrations on *Daphnia magna* acute toxicity in pharmaceutical industry wastewater after photocatalytic degradation process, at 30°C and at 60°C.

No	Parameters	***Daphnia magna* Acute Toxicity Values, * EC (mg/l)**							
		25°C							
		0. min		**60. min**		**120. min**		**180. min**	
		***EC_{50}**		***EC**		***EC**		***EC**	
1	Raw ww, control	850		EC_{45}=625		EC_{40}=370		EC_{29}=153	
		30°C				**60°C**			
		0. min	**60. min**	**120. min**	**180. min**	**0. min**	**60. min**	**120. min**	**180. min**
		***EC_{50}**	***EC**	***EC**	***EC**	***EC_{50}**	***EC**	***EC**	***EC**
2	Raw ww, control	850	EC_{39}= 468	EC_{34}= 228	EC_{23}= 111	850	EC_{34}= 373	EC_{29}= 210	EC_{18}= 71
3	SMM=5 mg/l	850	EC_{33}= 449	EC_{23}= 144	EC_{18}= 259	850	EC_{33}= 129	EC_{18}= 424	EC_{13}= 339
	OFX=10 mg/l	850	EC_{37}= 449	EC_{22}= 174	EC_{17}= 99	850	EC_{32}= 424	EC_{17}= 139	EC_{7}= 89
	OFX=20 mg/l	850	EC_{33}= 349	EC_{18}= 239	EC_{13}= 89	850	EC_{28}= 149	EC_{13}= 59	EC8= 374
	OFX=40 mg/l	850	EC_{43}= 299	EC_{28}= 169	EC_{23}= 51	850	EC_{38}= 249	EC_{23}= 109	EC_{18}= 10
* EC values were calculated based on COD_{dis} (mg/l).									

The EC_{50} values decreased to EC_{28} to EC_{13} and to EC_{8} after 60 min, 120 min and 180 min, respectively, in SMM=20 mg/l at 60°C (**Table 3: SET 3**). The EC_{28}, the EC_{13} and the EC_{8} values were measured as 149 mg/l, 59 mg/l and 374 mg/l, respectively, in SMM=20 mg/l at 60°C. The toxicity removal efficiencies were 53.83%, 83.51% and 93.27% after 60 min, 120 min and 180 min, respectively, in SMM=20 mg/l at 60°C (**Table 3: SET 3**). 93.27% maximum *Daphnia magna* acute toxicity removal was obtained in SMM=20 mg/l after 180 min and at 60°C, respectively (**Table 3: SET 3**).

The EC_{50} values decreased to EC_{38}=449 mg/l to EC_{23}=144 mg/l and to EC_{18}=259 mg/l after 60 min, 120 min and 180 min, respectively, in SMM=5 mg/l at 30°C (**Table 3: SET 3**). The EC_{50} values decreased to EC_{37}=449 mg/l to EC_{22}=174 mg/l and to EC_{17}=99 mg/l after 60 min, 120 min and 180 min, respectively, in SMM=10 mg/l and at 30°C. The EC_{50} values decreased to EC_{43}=299 mg/l to EC_{28}=169 mg/l and to EC_{23}=51 mg/l after 60 min, 120 min and 180 min, respectively, in SMM=40 mg/l and at 30°C. The *Daphnia magna* acute toxicity removals were 73.11%, 73.45% and 64.10% in 5 mg/l, 10 mg/l and 40 mg/l SMM, respectively, after

180 min and at 30°C. It was observed an inhibition effect of SMM=40 mg/l to *Daphnia magna* after 180 min and at 30°C (**Table 3: SET 3**).

The EC_{50} values decreased to EC_{33}=129 mg/l to EC_{18}=424 mg/l and to EC_{13}=339 mg/l after 60 min, 120 min and 180 min, respectively, in SMM=5 mg/l and at 60°C (**Table 3: SET 3**). The EC_{50} values decreased to EC_{32}=424 mg/l to EC_{17}=139 mg/l and to EC_{7}=89 mg/l after 60 min, 120 min and 180 min, respectively, in SMM=10 mg/l and at 60°C. The EC_{50} values decreased to EC_{38}=249 mg/l to EC_{23}=109 mg/l and to EC_{18}=10 mg/l after 60 min, 120 min and 180 min, respectively, in SMM=40 mg/l and at 60°C. The *Daphnia magna* acute toxicity removals were 84.95%, 93.54% and 74.22% in 5 mg/l, 10 mg/l and 40 mg/l SMM, respectively, after 180 min and at 60°C. It was observed an inhibition effect of SMM=40 mg/l to *Daphnia magna* after 180 min and at 60°C (**Table 3: SET 3**).

Increasing the SMM concentrations from 5 mg/l to 40 mg/l did not have a positive effect on the decrease of EC_{50} values as shown in **Table 3 at SET 3**. SMM concentrations > 20 mg/l decreased the acute toxicity removals by hindering the photocatalytic degradation process. Similarly, a significant contribution of increasing SMM concentration to acute toxicity removal at 60°C after 180 min of photocatalytic degradation time was not observed. Low toxicity removals found at high SMM concentrations could be attributed to their detrimental effect on the *Daphnia magna* (**Table 3: SET 3**).

3.9.3. Direct Effects of SMM Concentrations on the Acute Toxicity of Microtox (*Aliivibrio fischeri* or *Vibrio fischeri*) and *Daphnia magna* without Pharmaceutical Industry Wastewater after Photocatalytic Degradation Process

The acute toxicity test was performed in the samples containing 5 mg/l, 10 mg/l, 20 mg/l and 40 mg/l SMM concentrations, at 25°C room temperature. In order to detect the direct responses of Microtox (*Aliivibrio fischeri* or *Vibrio fischeri*) and *Daphnia magna* to the increasing SMM concentrations the toxicity test were performed without pharmaceutical industry wastewater after photocatalytic degradation process, at 25°C room temperature. The initial EC values and the the EC_{50} values were measured in the samples containing increasing SMM concentrations after 180 min photocatalytic degradation time. **Table 4** showed the responses of Microtox (*Aliivibrio fischeri* or *Vibrio fischeri*) and *Daphnia magna* to increasing SMM concentrations.

Table 4: The responses of Microtox (*Aliivibrio fischeri* or *Vibrio fischeri*) and *Daphnia magna* acute toxicity tests in addition of increasing SMM concentrations without phamaceutical industry wastewater during photocatalytic degradation process after 180 min photocatalytic degradation time, at 25°C room temperature.

SMM Conc. (mg/l)	Microtox (*Aliivibrio fischeri* or *Vibrio fischeri*) Acute Toxicity Test			*Daphnia magna* Acute Toxicity Test		
	Initial Acute Toxicity EC_{50} Value (mg/l)	Inhibitions after 180 min photocatalytic degradation time	EC Values (mg/l)	Initial Acute Toxicity EC_{50} Value (mg/l)	Inhibitions after 180 min photocatalytic degradation time	EC Values (mg/l)
5	EC_{11}= 23	-	-	EC_{11}= 38	-	-
10	EC_{15}= 78	3	EC_{2}= 3	EC_{20}= 98	5	EC_{3}= 4
20	EC_{21}= 148	6	EC_{4}= 6	EC_{31}= 198	7	EC_{7}= 10

40	EC_{26}= 218	8	EC_6= 9	EC_{41}= 298	10	EC_9= 14

The acute toxicity originating only from 5 mg/l, 10 mg/l, 20 mg/l and 40 mg/l SMM were found to be low (**Table 4**). 5 mg/l SMM did not exhibited toxicity to *Aliivibrio fischeri* (or *Vibrio fischeri*) and *Daphnia magna* before and after 180 min photocatalytic degradation time. The toxicity atributed to the 10 mg/l, 20 mg/l and 40 mg/l SMM were found to be low in the samples without pharmaceutical industry wastewater after photocatalytic degradation process for the test organisms mentioned above. The acute toxicity originated from the SMM decreased significantly to EC_2, EC_4 and EC_6 after 180 min photocatalytic degradation time. Therefore, it can be concluded that the toxicity originating from the SMM is not significant and the real acute toxicity throughout photocatalytic degradation process was attributed to the pharmaceutical industry wastewater, to their metabolites and to the photocatalytic degradation by-products (**Table 4**).

4. CONCLUSIONS

The maximum 99.6% SMM removal efficiency was obtained during photocatalytic degradation process in pharmaceutical industry wastewater, at 350 W UV-vis light irradiation power, at 147 mW/cm^2 light intensity, after 120 min photocatalytic degradation time, at pH=12.0 and at 25^{o}C, respectively.

The maximum 99.2% SMM removal efficieny was found with photocatalytic degradation process in pharmaceutical industry wastewater, at 5 mg/l SMM, at 350 W UV-vis irradiation power, at 147 mW/cm^2 light intensity, after 120 min photocatalytic degradation time, at pH=12.0 and at 25^{o}C, respectively.

The maximum 99.5% SMM removal efficieny was measured to 800 mg/l CuO/ZrO_2 NCs with photocatalytic degradation process in pharmaceutical industry wastewater, at 5 mg/l SMM, at 350 W UV-vis light irradiation power, at 147 mW/cm^2 light intensity, after 120 min photocatalytic degradation time, at pH=12.0 and at 25^{o}C, respectively.

The maximum 99.4% SMM removal efficiency was measured at 4/3wt CuO/ZrO_2 NCs mass ratios, at 5 mg/l SMM, at 800 mg/l CuO/ZrO_2 NCs, at 350 W UV-vis light irradiation power, at 147 mW/cm^2 light intensity, after 120 min photocatalytic degradation time, at pH=12.0 and at 25^{o}C, respectively.

The maximum 99.5% SMM recovery efficiency was measured in pharmaceutical industry wastewater during photocatalytic degradation process, after 1. recycle time, at 5 mg/l SMM, at 800 mg/l CuO/ZrO_2 NCs, at 4/3wt CuO/ZrO_2 NCs mass rartio, at 350 W UV-vis light irradiation power, at 147 mW/cm^2 light intensity, after 120 min photocatalytic degradation time, at pH=12.0 and at 25^{o}C, respectively.

97.31% maximum Microtox (*Aliivibrio fischeri*) acute toxicity removal yield was found in SMM=20 mg/l after 180 min and at 60^{o}C. It was observed an inhibition effect of SMM=40 mg/l to Microtox with *Vibrio fischeri* after 180 min, and at 60^{o}C. 93.27% maximum *Daphnia magna* acute toxicity removal was obtained in SMM=20 mg/l after 180 min and at 60^{o}C, respectively. It was obtained an inhibition effect of SMM=40 mg/l to *Daphnia magna* after 180 min and at 60^{o}C. Increasing the SMM concentrations from 5 mg/l to 40 mg/l did not have a positive effect on the decrease of EC_{50} values. SMM concentrations > 20 mg/l decreased the acute toxicity removals by hindering the photocatalytic degradation process. Similarly, a significant contribution of increasing SMM concentration to acute toxicity removal at 60^{o}C after 180 min of photocatalytic degradation time was not observed. Low toxicity removals found at high SMM concentrations could be attributed to their detrimental effect on *Aliivibrio fischeri* and *Daphnia magna.*

As a result, the CuO/ZrO_2 NCs photocatalyst during photocatalytic degradation process in pharmaceutical industry wastewater was stable in harsh environments such as acidic, alkaline, saline, and then was still effective process. When the amount of contaminant was increased, the a novel CuO/ZrO_2 NCs photocatalys during photocatalytic degradation process performance was still considerable. The synthesis and optimization of CuO/ZrO_2 heterostructure photocatalyst provides insights into the effects of preparation conditions on the material's characteristics and performance, as well as the application of the effectively designed photocatalyst in the removal of antibiotics, which can potentially be deployed for purifying wastewater, especially pharmaceutical wastewater. Finally, the combination of a simple, easy operation preparation process, excellent performance and cost effective, makes this CuO/ZrO_2 NCs a promising option during photocatalytic degradation process in pharmaceutical industry wastewater treatment.

REFERENCES

Aadil, M., Rahman, A., Zulfiqar, S., Alsafari, I.A., Shahid, M., Shakir, I., Agboola, P.O., Haider, S., Warsi, M.F. Facile synthesis of binary metal substituted copper oxide as a solar light driven photocatalyst and antibacterial substitute. Advanced Powder Technology. 2021;32(3):940-950.

Abul Kareem Alghurabi, M.N., Shakir Mahmood, R., Salim, E.T., Hamza Alhasan, S.F., Khalid, F.G. Structure, optical, and morphological investigations of nano copper oxide prepared using RPLD at different laser wavelength effects. Materials Today: Proceedings. 2021;42:2497-2501.

Ahammad, N.A., Zulkifli, M.A., Ahmad, M.A., Hameed, B.H., Mohd Din, A.T. Desorption of chloramphenicol from ordered mesoporous carbonalginate beads: Effects of operating parameters, and isotherm, kinetics, and regeneration studies. J. Environ. Chem. Eng., 2021;9:105015.

Ahmed, M.B., Zhou, J.L, Ngo, H.H., Guo, W. Adsorptive removal of antibiotics from water and wastewater: Progress and challenges. Sci. Total Environ., 2015;532:112-126.

Ahmed, M.B., Zhou, J.L., Ngo, H.H., Guo, W., Johir, M.A.H., Sornalingam, K., Belhaj, D., Kallel, M. Nano-Fe^0 immobilized onto functionalized biochar gaining excellent stability during sorption and reduction of chloramphenicol via transforming to reusable magnetic composite. Chem. Eng. J., 2017;322:571-581.

Ahmed, M.M., Brienza, M., Goetz, V., Chiron, S. Solar photo-fenton using peroxymonosulfate for organic micropollutants removal from domestic wastewater: Comparison with heterogeneous TiO_2 photocatalysis. Chemosphere, 2014;117:256-261.

Ahmed, W., Iqbal, J. Co doped ZrO_2 nanoparticles: An efficient visible light triggered photocatalyst with enhanced structural, optical and dielectric characteristics. Ceram. Int. 2020;46:25833–25844.

Akyon, B., McLaughlin, M., Hernández, F., Blotevogel, J., Bibby, K. Characterization and biological removal of organic compounds from hydraulic fracturing produced water. Environ. Sci. Process., 2019;21:279-290.

Alagha, O., Ouerfelli, N., Kochkar, H., Almessiere, M.A., Slimani, Y., Manikandan, A., Baykal, A., Mostafa, A., Zubair, M., Barghouthi, M.H. Kinetic modeling for photo-assisted penicillin G degradation of (Mn0.5Zn0.5)[CdxFe2-x]O4 ($x \leq 0.05$) nanospinel ferrites. Nanomaterials, 2021;11:970-986.

Aldeen, E.S., Jalil, A.A., Mim, R.S., Alhebshi, A., Hassan, N.S., Saravanan, R. Altered zirconium dioxide based photocatalyst for enhancement of organic pollutants degradation: A review. Chemosphere 2022;304:135349.

Alhazime, A.A. Effect of nano CuO doping on structural, thermal and optical properties of PVA/PEG blend. J Inorg Organomet Polym Mater., 2020;30(11):4459-4467

ALOthman, Z.A., Badjah, A.Y., Alharbi, O.M.L., Ali, I. Synthesis of chitosan composite iron nanoparticles for removal of diclofenac sodium drug residue in water. Int. J. Biol. Macromol., 2020;159:870-876.

Alygizakis, N.A., Gago-Ferrero, P., Borova, V.L., Pavlidou, A., Hatzianestis, I., Thomaidis, N.S. Occurrence and spatial distribution of 158 pharmaceuticals, drugs of abuse and related metabolites in offshore seawater. Sci. Total Environ., 2016;541:1097-1105.

Anjali, R., Shanthakumar, S. Insights on the current status of occurrence and removal of antibiotics in wastewater by advanced oxidation processes. J. Environ. Manage., 2019;246:51-62.

Arenas, N.E., Melo, V.M. Producción pecuaria y emergencia de antibiótico resistencia en Colombia: Revisión sistemática. Infectio, 2018;22:110-119.

Aslani A. Controlling the morphology and size of CuO nanostructures with synthesis by solvo/hydrothermal method without any additives. Physica B: Condensed Matter. 2011;406(2):150-154.

Avcu, T., Üner, O., Geçgel, Ü. Adsorptive removal of diclofenac sodium from aqueous solution onto sycamore ball activated carbon-isotherms, kinetics, and thermodynamic study. Surf. Interfaces., 2021;24:101097.

Babu, M.H., Podder, J., Dev, B.C., Sharmin, M. p to n-type transition with wide blue shift optical band gap of spray synthesized Cd doped CuO thin films for optoelectronic device applications. Surfaces and Interfaces. 2020;19:100459.

Bagheri, S., TermehYousefi, S.A., Do, T.-O. Photocatalytic pathway toward degradation of environmental pharmaceutical pollutants: Structure, kinetics and mechanism approach. Catal. Sci. Technol., 2017;7:4548-4569.

Bao, J., Zhu, Y., Yuan, S., Wang, F., Tang, H., Bao, Z., Zhou, H., Chen, Y. Adsorption of tetracycline with reduced graphene oxide decorated with $MnFe_2O_4$ nanoparticles. Nanoscale Res. Lett., 2018;13:396-403.

Baran, W., Sochacka, J., Wardas, W., 2006. Toxicity and biodegradability of sulfonamides and products of their photocatalytic degradation in aqueous solutions. Chemosphere, 2006;65:1295-1299

Barber, L.B., Keefe, S.H., LeBlanc, D.R., Bradley, P.M., Chapelle, F.H., Meyer, M.T., Loftin, K.A., Kolpin, D.W., Rubio, F. Fate of sulfamethoxazole, 4-nonylphenol, and 17b-estradiol in groundwater contaminated by wastewater treatment plant effluent. Environ. Sci. Technol., 2009;43:4843-4850.

Barry, S. Dangerously high levels of antibiotics found in world's major rivers, says study. World news global study, Euronews, 2019;1:1-10.

Batt, A.L., Snow, D.D., Aga, D.S. Occurrence of sulfonamide antimicrobials in private water wells in Washington County, Idaho, USA. Chemosphere, 2006;64:1963-1971.

Bellamkonda, S., Thangavel, N., Hafeez, H.Y., Neppolian, B., Ranga Rao, G. Highly active and stable multi-walled carbon nanotubes-graphene-TiO_2 nanohybrid: An efficient non-noble metal photocatalyst for water splitting. Catal. Today., 2019;321-322:120-127.

Biancullo, F., Moreira, N.F.F., Ribeiro, A.R., Manaia, C.M., Faria, J.L., Nunes, O.C., Castro-Silva, S.M., Silva, A.M.T. Heterogeneous photocatalysis using UVA-LEDs for the removal of antibiotics and antibiotic resistant bacteria from urban wastewater treatment plant effluents. Chem. Eng. J., 2019;367:304-313.

Boltaev GS, Ganeev RA, Krishnendu PS, Zhang K, Guo C. Nonlinear optical characterization of copper oxide nanoellipsoids. Sci Rep. 2019;9(1):11414.

Camacho-Munoz, D., Martín, J., Santos, J.L., Aparicio, I., Alonso, E. Concentration evolution of pharmaceutically active compounds in raw urban and industrial wastewater. Chemosphere, 2014;111:70-79.

Casanova, L.M., Sobsey, M.D. Antibiotic-resistant enteric bacteria in environmental waters. Water, 2016;8(12):561-567.

Chen, Y., Yang, J., Zeng, L., Zhu, M. Recent progress on the removal of antibiotic pollutants using photocatalytic oxidation process. Crit. Rev. Environ. Sci. Technol., 2022;52(8):1401-1448.

Cuerda-Correa, E.M., Alexandre-Franco, M.F., Fernandez-Gonzalez, C. Advanced oxidation processes for the removal of antibiotics from water, an overview. Water., 2020;12(1):102-153.

Cui, G., Guo, J., Zhang, Y., Zhao, Q., Fu, S., Han, T., Zhang, S., Wu, Y. Chitosan oligosaccharide derivatives as green corrosion inhibitors for P110 steel in a carbon-dioxide-saturated chloride solution. Carbohydr. Polym., 2019;203:386-395.

de Souza Santos, L.V., Meireles, A.M., Lange, L.C. Degradation of antibiotics norfloxacin by fenton, UV and UV/H_2O_2. J. Environ. Manag., 2015;154:8-12.

Dehghan, A., Mohammadi, A.A., Yousefi, M., Najafpoor, A.A., Shams, M., Rezania, S. Enhanced kinetic removal of ciprofloxacin onto metal-organic frameworks by sonication, process optimization and metal leaching study. Nanomaterials, 2019;9(10):1422-1438.

Dhineshbabu, N.R., Rajendran, V., Nithyavathy, N., Vetumperumal, R. Study of structural and optical properties of cupric oxide nanoparticles. Applied Nanoscience. 2015;6(6):933- 939.

Dietze, J.E., Scribner, E.A., Meyer, M.T., Kolpin, D.W. Occurrence of antibiotics in water from 13 fish hatcheries, 2001-2003. Int. J. Environ. An., 2005;85:1141-1152

Dinh, Q.T., Moreau-Guigon, E., Labadie, P., Alliot, F., Teil, M.-J., Blanchard, M., Chevreuil, M. Occurrence of antibiotics in rural catchments. Chemosphere, 2017;168:483-490.

Długosz, O., Szostak, K., Staroń, A., Pulit-Prociak, J., Banach, M. Methods for reducing the toxicity of metal and metal oxide NPs as biomedicine. Materials (Basel)., 2020;13(2):279.

Dong, D., Zhang, L., Liu, S., Guo, Z., Hua, X. Antibiotics in water and sediments from Liao River in Jilin Province, China: occurrence, distribution, and risk assessment. Environ. Earth Sci., 2016;75(16):1202, ref.45.

Eckenfelder, W.W., Industrial Water Pollution Control (2nd ed), Signapore: McGraw-Hill Inc.,1989.

Eddy, D.R., Puri, F.N., Noviyanti, A.R. Synthesis and photocatalytic activity of silica-based sand quartz as the supporting TiO_2 photocatalyst. Proced. Chem., 2015;17:55-58.

Falyouna, O., Idham, M.F., Maamoun, I., Bensaida, K., Ashik, U.P.M., Sugihara, Y., Eljamal, O. Promotion of ciprofloxacin adsorption from contaminated solutions by oxalate modified nanoscale zerovalent iron particles. J. Mol. Liq., 2022a;359:119323.

Falyouna, O., Maamoun, I., Bensaida, K., Tahara, A., Sugihara, Y., Eljamal, O. Encapsulation of iron nanoparticles with magnesium hydroxide shell for remarkable removal of ciprofloxacin from contaminated water. J. Colloid Interface Sci., 2022b;605:813-827.

Fekadu, S., Alemayehu, E., Dewil, R., Van der Bruggen, B. Pharmaceuticals in freshwater aquatic environments: a comparison of the african and european challenge. Sci. Total Environ., 2019;654:324-337.

Ferri, M., Ranucci, E., Romagnoli, P., Giaccone, V. Antimicrobial resistance: A global emerging threat to public health systems. Crit. Rev. Food Sci., 2017;57:2857-2876.

Fridkin, S., Baggs, J., Fagan, R., Magill, S., Pollack, L.A., Malpiedi, P., Slayton, R., Khader, K., Rubin, M.A., Jones, M., Samore, M.H., Dumyati, G., Dodds-Ashley, E., Meek, J.,

Yousey-Hindes, K., Jernigan, J., Shehab, N., Herrera, R., McDonald, C.L., Schneider, A., Srinivasan, A. Vital signs: improving antibiotic use among hospitalized patients. MMWR-Morb. Mortal. Wkly. Rep., 2014;63(9):194-200.

García-Galan, M.J., Díaz-Cruz, M.S., Barcelo, D. Determination of 19 sulfonamides in environmental water samples by automated on-line solid-phase extraction-liquid chromatography-tandem mass spectrometry (SPE-LC-MS/ MS). Talanta, 2010a;81:355-366.

García-Galan, M.J., Garrido, T., Fraile, J., Ginebreda, A., Díaz-Cruz, M.S., Barcelo, D. Simultaneous occurrence of nitrates and sulfonamide antibiotics in two ground water bodies of Catalonia (Spain). J. Hydrol., 2010b;383:93-101

García-López, E., Marcì, G., Pomilla, F., Paganini, M., Gionco, C., Giamello, E., Palmisano, L. ZrO_2 Based materials as photocatalysts for 2-propanol oxidation by using UV and solar light irradiation and tests for CO_2 reduction. Catal. Today, 2018;313:100–105.

Gerawork, M. Photodegradation of methyl orange dye by using Zinc Oxide–Copper Oxide nanocomposite. Optik., 2020;216:164864.

Görmez, F., Görmez, Ö., Gözmen, B., Kalderis, D. Degradation of chloramphenicol and metronidazole by electro-fenton process using graphene oxide Fe_3O_4 as heterogeneous catalyst. J. Environ. Chem. Eng., 2019;7:102990.

Guerrero-Araque, D., Acevedo-Peña, P., Ramírez-Ortega, D., Calderon, H.A., Gómez, R. Charge transfer processes involved in photocatalytic hydrogen production over $CuO/ZrO_2–TiO_2$ materials. Int. J. Hydrog. Energy., 2017a;42(15):9744-9753.

Guerrero-Areque, D., Gomez, R., Calderon, H.A. TEM Characterization of heterojunctions for photocatalytic application: ZrO_2-TiO_2 and CuO/ZrO_2-TiO_2. Microsc. Microanal., 2017b;23(S1):2036-2037.

Homem, V., Santos, L. Degradation and removal methods of antibiotics from aqueous matrices-A review. J. Environ. Manage., 2011;92(10):2304-2347.

Hu, L., Flanders, P.M., Miller, P.L., Strathmann, T.J., 2007. Oxidation of sulfamethoxazole and related antimicrobial agents by TiO2 photocatalysis. Water Res. 2007;41:2612-2626.

Hui, S.J., Lan, F.J., Hui, S.S., Qing, P.I.Y., Ke, S.M., Yan, S. (2012) Degradation of the antibiotic sulfamonomethoxine sodium in aqueous solution by photo-Fenton oxidation. Environ. Sci. Technol., 2012;57:558–564.

Huo, T.I. The first case of multidrug-resistant NDM−1-harboring Enterobacteriaceae in Taiwan: here comes the superbacteria! J. Chin. Med. Assoc., 2010;73:557-558.

Idham, M.F., Abdullah, B., Yusof, K.M. Effects of two cycle heat treatment on the microstructure and hardness of ductile iron. Pertanika. J. Sci. Technol., 2017;25:99-106.

Idham, M.F., Falyouna, O., Eljamal, O. Effect of graphene oxide synthesis method on the adsorption performance of pharmaceutical contaminants. Proc. Int. Exch. Innov. Conf. Eng. Sci., 2021;7:232-239.

Iqbal, M., Thebo, A.A., Shah, A.H., Iqbal, A., Thebo, K.H., Phulpoto, S.N, Mohsin, M.A. Influence of Mn-doping on the photocatalytic and solar cell efficiency of CuO nanowires. Inorg. Chem. Commun., 2017;76:71-76.

Ji, Y., Zhang, C., Zhang, X.J., Xie, P.F., Wu, C., Jiang, L. A high adsorption capacity bamboo biochar for CO_2 capture for low temperature heat utilization. Sep. Purif. Technol., 2022;293:121131.

Jiang, Q., Zhang, Y., Jiang, S., Wang, Y., Li, H., Han, W., Qu, J., Wang, L., Hu, Y. Graphene-like carbon sheetsupported nZVI for efficient atrazine oxidation degradation by persulfate activation. Chem. Eng. J., 2020;403:126309.

Jiménez-Tototzintle, M., Ferreira, I.J., da Silva Duque, S., Guimarães Barrocas, P.R., Saggioro, E.M. Removal of contaminants of emerging concern (CECs) and antibiotic

resistant bacteria in urban wastewater using UVA/TiO_2/H_2O_2 photocatalysis. Chemosphere, 2018;210:449-457.
Jung, A., Cho, S., Cho, W.J., Lee, K.-H. Morphology-controlled synthesis of CuO nano- and microparticles using microwave irradiation. Korean J. Chem. Eng. 2011;29(2):243-248.
Karthikeyan, K.G., Meyer, M.T. Occurrence of antibiotics in wastewater treatment facilities in Wisconsin, USA., Sci. Total Environ., 2006;361:196-207.
Karuppannan, S.K., Ramalingam, R., Mohamed Khalith, S.B., Musthafa, S.A., Dowlath, M.J.H., Munuswamy-Ramanujam, G., Arunachalam, K.D. Copper oxide nanoparticles infused electrospun polycaprolactone/gelatin scaffold as an antibacterial wound dressing. Mater. Lett., 2021;294:129787.
Kerrigan, J.F., Sandberg, K.D., Engstrom, D.R., LaPara, T.M., Arnold, W.A. Small and large-scale distribution of four classes of antibiotics in sediment: association with metals and antibiotic resistance genes. Environ. Sci. Process. Impacts., 2018;20:1167-1179.
Khalil, A.M.E., Memon, F.A., Tabish, T.A., Salmon, D., Zhang, S., Butler, D. Nanostructured porous graphene for efficient removal of emerging contaminants (pharmaceuticals) from water. Chem. Eng. J., 2020;398:125440.
Kim, S., Aga, D.S. Potential ecological and human health impacts of antibiotics and antibiotic-resistant bacteria from wastewater treatment plants. J. Toxicol. Environ. Health B, 2007;10:559-573.
Kumar, P., Chandra Mathpal, M., Prakash, J., Viljoen, B.C., Roos, W.D., Swart, H.C. Band gap tailoring of cauliflower-shaped CuO nanostructures by Zn doping for antibacterial applications. J. Alloys Compd., 2020;832:154968
Lange, B. LUMISmini, Operating Manual. Dusseldorf, Germany: Dr Bruno LANGE., 1994.
Lange, B. LUMIXmini type luminometer. Dusseldorf: Dr LANGE Company., 1996.
Lange, B. Vibrio fischeri -Microtox LCK 491 kit. Germany: Dr LANGE., 2010.
Le, T.X., Munekage, Y. Residues of selected antibiotics in water and mud from shrimp ponds in mangrove areas in Viet Nam. Mar. Pollut. Bull., 2004;49:922-929.
Li, H., Hu, J., Meng, Y., Su, J., Wang, X. An investigation into the rapid removal of tetracycline using multilayered graphene-phase biochar derived from waste chicken feather. Sci. Total Environ., 2017a;603-604:39-48.
Li, X., Zhu, W., Lu, X., Zuo, S., Yao, C., Ni, C. Integrated nanostructures of CeO_2 /attapulgite/g-C_3N_4 as efficient catalyst for photocatalytic desulfurization: Mechanism, kinetics and influencing factors. Chem. Eng. J., 2017b;326:87-98.
Li, Y., Gutiérrez Moreno, J.J., Song, Z., Liu, D., Wang, M., Ramiere, A., Feng, Z., Niu, Q.J., Sasaki, T., Cai, X. Controlled synthesis of perforated oxide nanosheets with high density nanopores showing superior water purification performance. ACS Appl. Mater. Interfaces., 2022;14:18513-18524.
Lima, V.B., Goulart, L.A., Rocha, R.S., Steter, J.R., Lanza, M.R.V. Degradation of antibiotic ciprofloxacin by different AOP systems using electrochemically generated hydrogen peroxide. Chemosphere, 2020;247:125807.
Lin, A.Y.-C., Yu, T.-H., Lin, C.-F. Pharmaceutical contamination in residential, industrial, and agricultural waste streams: risk to aqueous environments in Taiwan. Chemosphere, 2008;74:131-141.
Lipps, W.C., Braun-Howland, E.B., Baxter, T.E. (2022). Standard Methods for the Examination of Water and Wastewater. (24th. Edition). Lipps, W.C., Braun-Howland, E.B., Baxter, T.E. (editors), American Public Health Association (APHA), American Water Works Association (AWWA), Water Environment Federation (WEF), Elevate Your Standards. American Public Health Association 800 I Street, NW Washington DC: 20001-3770, USA, December 1, 2022; ISBN:9780875532998.

Littlefield, N.A., Gaylor, D.W., Blackwell, B.N., Allen, R.R. Chronic toxicity/carcinogenicity studies of sulfamethazine in B6C3F1 mice. Food. Chem. Toxicol., 1989;27:455–463

Littlefield, N.A., Sheldon, W.G., Allen, R., Gaylor, D.W. Chronic toxicity/carcinogenicity studies of sulfamethazine in Fischer 344/N rats: two-generation exposure. Food. Chem. Toxicol., 1990;28:157–167.

Liu, J., Yin, M.L., Xiao, T.F., Zhang, C.S., Tsang, D.C.W., Bao, Z.A., Zhou, Y.T., Chen, Y.H., Luo, X.W., Yuan, W.H., Wang, J. Thallium isotopic fractionation in industrial process of pyrite smelting and environmental implications. J. Hazard. Mater., 2020;384(11):121378.

Liu, W., Li, Z., Kang, Q., Wen, L. Efficient photocatalytic degradation of doxycycline by coupling α-Bi_2O_3/g-C_3N_4 composite and H_2O_2 under visible light. Environ. Res., 2021a;197:110925.

Liu, Y.P., Lv, Y.-T., Guan, J.-F., Khoso, F.M., Jiang, X.-Y., Chen, J., Li, W.-J., Yu, J.-G. Rational design of three-dimensional graphene/graphene oxide-based architectures for the efficient adsorption of contaminants from aqueous solutions. J. Mol. Liq., 2021b;343:117709.

Liu, W.-X., Song, S., Ye, M.-L., Zhu, Y., Zhao, Y.-G., Lu, Y. Nanomaterials with excellent adsorption characteristics for sample pretreatment: a review. Nanomaterials., 2022;12:1845.

Lu, Y., Chu, Y., Zheng, W., Huo, M., Huo, H., Qu, J., Yu, H., Zhao, Y. Significant tetracycline hydrochloride degradation and electricity generation in a visible-light-driven dual photoelectrode photocatalytic fuel cell using $BiVO_4$/TiO_2 NT photoanode and Cu_2O/TiO_2 NT photocathode. Electrochim. Acta., 2019;320:134617

Lu, Z.Y., Ma, Y.L., Zhang, J.T., Fan, N.S., Huang, B.C., Jin, R.C. A critical review of antibiotic removal strategies: Performance and mechanisms. J. Water. Process. Eng., 2020;38:101681.

Luo, B., Xu, D., Li, D., Wu, G., Wu, M., Shi, W., Chen, M. Fabrication of a Ag/Bi_3TaO_7 plasmonic photocatalyst with enhanced photocatalytic activity for degradation of tetracycline. ACS Appl. Mater. Interfaces., 2015;7(31):17061-17069.

Luo, Y., Xu, L., Rysz, M., Wang, Y., Zhang, H., Alvarez, P.J.J. Occurrence and transport of tetracycline, sulfonamide, quinolone, and macrolide antibiotics in the Haihe River basin, China. Environ. Sci. Technol., 2011;45:1827-1833.

Mady, A.H., Baynosa, M.L., Tuma, D., Shim, J-J. Heterogeneous activation of peroxymonosulfate by a novel magnetic 3D gamma-MnO_2@$ZnFe_2O_4$/rGO nanohybrid as a robust catalyst for phenol degradation. Appl. Catal. B: Environ., 2019;244:946-956.

Majumdar, D., Ghosh, S. Recent advancements of copper oxide based nanomaterials for supercapacitor applications. J. Energy Storage., 2021;34:101995.

Masoudi, F., Kamranifar, M., Safari, F., Naghizadeh, A. Mechanism, kinetics and thermodynamic of Penicillin G antibiotic removal by silica nanoparticles from simulated hospital wastewater. Desalination Water Treat., 2019;169:333-341.

Maycock, D.S., Watts, C.D. Pharmaceuticals in drinking water. Encycl. Environ. Heal., 2011;472-484.

McConnell, M.M., Truelstrup Hansen, L., Jamieson, R.C., Neudorf, K.D., Yost, C.K., Tong, A. Removal of antibiotic resistance genes in two tertiary level municipal wastewater treatment plants. Sci. Total Environ., 2018;643:292-300.

Mokhati, A., Benturki, O., Bernardo, M., Kecira, Z., Matos, I., Lapa, N., Ventura, M., Soares, O.S.G.P., Botelho do Rego, A.M., Fonseca, I.M. Nanoporous carbons prepared from argan nutshells as potential removal agents of diclofenac and paroxetine. J. Mol. Liq., 2021;326:115368.

Nanda, B., Pradhan, A.C., Parida, K.M. Fabrication of mesoporous CuO/ZrO_2-MCM-41 nanocomposites for photocatalytic reduction of Cr(VI). Chem. Eng. J., 2017;316:1122-1135

Nguyen, C.H., Tran, M.L., Van Tran, T.T., Juang, R.S. Efficient removal of antibiotic oxytetracycline from water by fenton-like reactions using reduced graphene oxide-supported bimetallic Pd/nZVI nanocomposites. J. Taiwan Inst. Chem. Eng., 2021;119:80-89.

Nguyen, L.T., Nguyen, H.T., Pham, T.D., Tran, T.D., Chu, H.T., Dang, H.T., Van der Bruggen, B. UV–visible light driven photocatalytic degradation of ciprofloxacin by N, S co-doped TiO_2: the effect of operational parameters. Top. Catal., 2020;63(11):985-995.

Olthof, M., Eckenfelder, W.W. Coagulation of textile wastewater. Text. Chem. Color., 1976;8:18-22.

Pellerito, A., Ameen, S.M., Micali, M., Caruso, G. Antimicrobial substances for food packaging products: the current situation. J. AOAC. Int., 2018;101(4):942-947.

Phasuphan, W., Praphairaksit, N., Imyim, A. Removal of ibuprofen, diclofenac, and naproxen from water using chitosan-modified waste tire crumb rubber. J. Mol. Liq., 2019;294:111554.

Pi, Y., Feng, J., Sun, J., Sun, J. Facile, effective, and environmentfriendly degradation of sulfamonomethoxine in aqueous solution with the aid of a UV/Oxone oxidative process. Environ. Sci. Pollut. Res., 2013;20:8621–8628.

Pirzada, B.M., Mir, N.A., Qutub, N., Mehraj, O., Sabir, S., Muneer, M. Synthesis, characterization and optimization of photocatalytic activity of TiO_2/ZrO_2 nanocomposite heterostructures. Mater. Sci. Eng. B., 2015;193:137–145.

Qiao, D., Li, Z., Duan, J., He, X. Adsorption and photocatalytic degradation mechanism of magnetic graphene oxide/ZnO nanocomposites for tetracycline contaminants. Chem. Eng. J., 2020;400:125952.

Rachna, Rani, M., Shanker, U. Synergistic effects of zinc oxide coupled copper hexacyanoferrate nanocomposite: Robust visible-light driven dye degradation. J. Colloid Interface Sci., 2021;584:67-79.

Raizada, P., Sudhaik, A., Patial, S., Hasija, V., Parwaz Khan, A.A., Singh, P., Gautam, S. Kaur, M., Nguyen, V-H. Engineering nanostructures of CuO-based photocatalysts for water treatment: Current progress and future challenges. Arab. J. Chem., 2020;13(11):8424-8457.

Reel, J.R., Tyl, R.W., Lawton, A.D., Lamb, J.C. Reproductive toxicity of sulfamethazine in Swiss CD-1 mice during continuous breeding. Fundam. Appl. Toxicol., 1992;18:609–615

Ren, Y., Lin, L., Ma, J., Yang, J., Feng, J., Fan, Z. Sulfate radicals induced from peroxymonosulfate by magnetic ferrospinel MFe_2O_4 (M ¼ Co, Cu, Mn, and Zn) as heterogeneous catalysts in the water. Appl. Catal. B: Environ., 2015;165:572-578.

Renuka, L., Anantharaju, K.S., Vidya, Y.S., Nagaswarupa, H.P., Prashantha, S.C., Sharma, S.C., Nagabhushana, H., Darshan, G.P. A simple combustion method for the synthesis of multi-functional ZrO_2/CuO nanocomposites: Excellent performance as Sunlight photocatalysts and enhanced latent fingerprint detection. Appl. Catal. B: Environ., 2017;210:97-115.

Rigueto, C.V.T., Rosseto, M., Nazari, M.T., Ostwald, B.E.P., Alessandretti, I., Manera, C., Piccin, J.S., Dettmer, A. Adsorption of diclofenac sodium by composite beads prepared from tannery wastesderived gelatin and carbon nanotubes. J. Environ. Chem. Eng., 2021;9:105030.

Ryan, C.C., Tan, D.T., Arnold, W.A. Direct and indirect photolysis of sulfamethoxazole and trimethoprim in wastewater treatment plant effluent. Water Res., 2011;45:1280-1286.

Sahu, K., Singhal, R., Mohapatra, S. Morphology Controlled CuO Nanostructures for efficient catalytic reduction of 4-nitrophenol. Catal Letters., 2019;150(2):471-481.
Shahnaz, T., Vishnu Priyan, V., Pandian, S., Narayanasamy, S. Use of nanocellulose extracted from grass for adsorption abatement of ciprofloxacin and diclofenac removal with phyto, and fish toxicity studies. Environ. Pollut., 2021;268:115494.
Shan, D., Deng, S., Li, J., Wang, H., He, C., Cagnetta, G., Wang, B., Wang, Y., Huang, J., Yu, G. Preparation of porous graphene oxide by chemically intercalating a rigid molecule for enhanced removal of typical pharmaceuticals. Carbon. N. Y., 2017;119:101-109.
Shirani, Z., Song, H., Bhatnagar, A. Efficient removal of diclofenac and cephalexin from aqueous solution using Anthriscus sylvestris-derived activated biochar. Sci. Total. Environ., 2020;745:140789.
Siedlewicz, G., Białk-Bielinska, A., Borecka, M., Winogradow, A., Stepnowski, P., Pazdro, K. Presence, concentrations and risk assessment of selected antibiotic residues in sediments and near-bottom waters collected from the Polish Coastal Zone in the Southern Baltic Sea-Summary of 3years of studies. Mar. Pollut. Bull., 2018;129:787-801.
Sohail, M.I., Ayub, M.A., Ziaur Rehman, M., Azhar, M., Farooqi, Z.U.R., Siddiqui, A., et al. Chapter 7-Sufficiency and toxicity limits of metallic oxide nanoparticles in the biosphere. In: Tahir MB, Sagir M, Asiri AM, editors. Nanomaterials: Synthesis, Characterization, Hazards and Safety: Elsevier; 2021:145-221.
Statgraphics Centurion XV, sofware, StatPoint Inc, Statgraphics Centurion XV, Herndon, VA, USA, 2005.
Sturini, M., Puscalau, C., Guerra, G., Maraschi, F., Bruni, G., Monteforte, F., Profumo, A., Capsoni, D. Combined layer-by-layer/hydrothermal synthesis of Fe_3O_4@MIL-100(Fe) for ofloxacin adsorption from environmental waters. Nanomaterials., 2021;11:3275.
Sukul, P., Lamshoft, M., Zühlke, S., Spiteller, M. Sorption and desorption of sulfadiazine in soil and soil-manure systems. Chemosphere, 2008;73:1344e1350
Sukul, P., Spiteller, M. Sulfonamides in the environment as veterinary drugs. Rev. Environ. Contam. Toxicol., 2006;187:67-101
Sun, L., Cao, G., Xu, M., Cheng, G., Xia, D., Yuan, X., Liu, J. Visible-light-induced peroxymonosulfate activation over $ZnFe_2O_4$ fine nanoparticles for ofloxacin degradation. Elementa: Science of the Anthropocene., 2021b;9(1):1-10.
Sun, T., Fan, R., Zhang, J., Qin, M., Chen, W., Jiang, X., Zhu, K., Ji, C., Hao, S., Yang, Y. Stimuli-Responsive metal–organic framework on a metal–organic framework heterostructure for efficient antibiotic detection and anticounterfeiting. ACS Appl. Mater. Interfaces., 2021a;13:35689-35699.
Tamma, P.D., Avdic, E., Li, D.X., Dzintars, K., Cosgrove, S.E. Association of adverse events with antibiotic use in hospitalized patients. JAMA Intern. Med., 2017;177:1308-1315.
Tamtam, F., Mercier, F., Le Bot, B., Eurin, J., Tuc Dinh, Q., Clement, M., Chevreuil, M. Occurrence and fate of antibiotics in the Seine River in various hydrological conditions. Sci. Total Environ., 2008;393:84-95.
Tamtam, F., van Oort, F., Le Bot, B., Dinh, T., Mompelat, S., Chevreuil, M., Lamy, I., Thiry, M. Assessing the fate of antibiotic contaminants in metal contaminated soils four years after cessation of long-term waste water irrigation. Sci. Total Environ., 2011;09:540-547.
Tan, L., Li, L.Y., Ashbolt, N., Wang, X.L., Cui, Y.X., Zhu, X., Xu, Y., Yang, Y., Mao, D.Q., Luo, Y. Arctic antibiotic resistance gene contamination, a result of anthropogenic activities and natural origin. Sci. Total Environ., 2018;621:1176-1184.

Tang, H., Li, W., Jiang, H., Lin, R., Wang, Z., Wu, J., He, G., Shearing, P.R., Brett, D.J.L. ZIF-8-derived hollow carbon for efficient adsorption of antibiotics. Nanomaterials, 2019;9:117.

Thiele-Bruhn, S. Pharmaceutical antibiotic compounds in soils-a review. J. Plant Nutr. Soil Sci., 2003;166:145-167.

Tong, S., Pan, J., Lu, S., Tang, J. Patient compliance with antimicrobial drugs: a Chinese survey. Am. J. Infect. Control., 2018;46:E25-E29.

Wang, J, Zhuan, R. Degradation of antibiotics by advanced oxidation processes: An overview. Sci. Total. Environ., 2020;701:135023.

Wang, Z.T., Xu, J.L., Zhou, H., Zhang, X. Facile synthesis of Zn(II)-doped g-C_3N_4 and their enhanced photocatalytic activity under visible light irradiation. Rare. Met., 2019a;38(5):459-467.

Wang, B., Zhu, B., Yun, S., Zhang, W., Xia, C., Afzal, M., Cai, Y., Liu, Y., Wang, Y., Wang, H. Fast ionic conduction in semiconductor CeO_2-δ electrolyte fuel cells. NPG Asia Mater., 2019b;11:51.

Wang, J., Hao, J., Liu, D., Qin, S., Chen, C., Yang, C., Liu, Y., Yang, T., Fan, Y., Chen, Y., Lei, W. Flower stamen-like porous boron carbon nitride nanoscrolls for water cleaning. Nanoscale., 2017a;9:9787-9791.

Wang, X., Wang, A., Lu, M., Ma, J. Synthesis of magnetically recoverable Fe^0/graphene-TiO_2 nanowires composite for both reduction and photocatalytic oxidation of metronidazole. Chem. Eng. J., 2017b;337:372–384.

Wang, W., Zhu, Q., Dai, Q., Wang, X. Fe doped CeO_2 nanosheets for catalytic oxidation of 1,2-dichloroethane: effect of preparation method. Chem. Eng. J., 2017c;307:1037-1046.

Wang, Y., Sun, H., Ang, H.M., Tade, M.O., Wang, S. Facile synthesis of hierarchically structured magnetic MnO_2/$ZnFe_2O_4$ hybrid materials and their performance in heterogeneous activation of peroxymonosulfate. ACS Appl. Mater. Interfaces., 2014;6(22):19914-19923.

Wang, Z., Song, L., Wang, Y., Zhang, X.F., Yao, J. Construction of a hybrid graphene oxide/nanofibrillated cellulose aerogel used for the efficient removal of methylene blue and tetracycline. J. Phys. Chem. Solids., 2021;150:109839.

Wei, Z., Liu, J., Shangguan, W. A review on photocatalysis in antibiotic wastewater: Pollutant degradation and hydrogen production. Chinese J. Catal. 2020;41(10):1440-1450.

Yadav, S., Asthana, A., Singh, A.K., Chakraborty, R., Vidya, S.S., Singh, A., Carabineiro, S.A.C. Methionine-functionalized graphene oxide/sodium alginate bio-polymer nanocomposite hydrogel beads: synthesis, ısotherm and kinetic studies for an adsorptive removal of fluoroquinolone antibiotics. Nanomaterials, 2021;11(3):568-593.

Yan, J., Lei, M., Zhu, L., Anjum, M.N., Zou, J., Tang, H. Degradation of sulfamonomethoxine with Fe_3O_4 magnetic nanoparticles as heterogeneous activator of persulfate. J. Hazard. Mater., 2011;186:1398–1404.

Yang, L., Zhu, Y.-J., He, G., Li, H., Tao, J.-C. multifunctional photocatalytic filter paper based on ultralong nanowires of the calcium-alendronate complex for high-performance water purification. ACS Appl. Mater. Interfaces., 2022;14:9464-9479.

Yang, X., Chen, Z., Zhao, W., Liu, C., Qian, X., Zhang, M., Wei, G., Khan, E., Hau Ng, Y., Sik Ok, Y. Recent advances in photodegradation of antibiotic residues in water. Chem. Eng. J., 2021;405:126806.

Yu, F., Sun, S., Han, S., Zheng, J., Ma, J. Adsorption removal of ciprofloxacin by multi-walled carbon nanotubes with different oxygen contents from aqueous solutions. Chem. Eng. J., 2016;285:588-595.

Yu, H., Wang, D., Zhao, B., Lu, Y., Wang, X., Zhu, S., Qin, W., Huo, M. Enhanced photocatalytic degradation of tetracycline under visible light by using a ternary

photocatalyst of Ag_3PO_4/AgBr/g-C_3N_4 with dual Z-scheme heterojunction. Separ. Purif. Tech., 2020;237:116365.

Zar, J.H. Biostatistical analysis, Prentice-Hall, Englewood Cliffs, 1984.

Zeidman, A.B., Rodriguez-Narvaez, O.M., Moon, J., Bandala, E.R. Removal of antibiotics in aqueous phase using silica-based ımmobilized nanomaterials: a review. Environ. Technol. Innov., 2020;20:101030.

Zhang, C., Li, Y., Shuai, D., Shen, Y., Xiong, W., Wang, L. Graphitic carbon nitride (g-C_3N_4)-based photocatalysts for water disinfection and microbial control: A review. Chemosphere, 2019;214:462-479.

Zhang, X., Lou, S., Zeng, Y. Facile fabrication of a novel visible light active g-C_3N_4-$CoMoO_4$ heterojunction with largely improved photocatalytic performance. Mater. Lett., 2020a;281:128661.

Zhang, W., Mohamed, A.R., Ong, W.-J. Z-scheme photocatalytic systems for carbon dioxide reduction: where are we now? Angew. Chem. Int. Ed., 2020b;59(51):22894-22915.

Zhang, K., Zhou, M., Yu, C., Yang, K., Li, X., Dai, W., Guan, J., Shu, Q., Huang, W. Construction of S-scheme g-C_3N_4/ZrO_2 heterostructures for enhancing photocatalytic disposals of pollutants and electrocatalytic hydrogen evolution. Dyes Pigm., 2020c;180:108525.

Zhang, L.-H., He, Y.-W., Chen, M., Gao, M., Qiu, T.-L., Wang, X.-M. Pollution characteristics of antibiotic resistant bacteria from atmospheric environment of animal feeding operations. Huan. Jing. Ke. Xue., 2016;37:4531-4537.

Zhao, H., Liu, X., Cao, Z., Zhan, Y., Shi, X., Yang, Y., Zhou, J., Xu, J. Adsorption behavior and mechanism of chloramphenicols, sulfonamides, and nonantibiotic pharmaceuticals on multi-walled carbon nanotubes. J. Hazard. Mater., 2016;310:235-245.

Zhao, J., Yang, X., Liang, G., Wang, Z., Li, S., Wang, Z., Xie, X. Effective removal of two fluoroquinolone antibiotics by PEG-4000 stabilized nanoscale zerovalent iron supported onto zeolite (PZ-NZVI). Sci. Total Environ., 2020;710:136289.

Zhong, Y., Han, L., Yin, X., Li, H., Fang, D., Hong, G. Three dimensional functionalized carbon/tin(IV) sulfide biofoam for photocatalytical purification of chromium(VI)-containing wastewater. ACS Sustain. Chem. Eng., 2018;6:10660-10667.

Zhu, A., Zhu, W., Wub, Z., Jing, Y. Recovery of clindamycin from fermentation wastewater with nanofiltration membranes. Water Res., 2003;37(15):3718-3732.

Zhu, S., Xu, Y., Zhu, Z., Liu, Z., Wang, W. Activation of peroxymonosulfate by magnetic Co-Fe/SiO_2 layered catalyst derived from iron sludge for ciprofloxacin degradation. Chem. Eng. J., 2020;384:123298.